THE PENNSYLVANIA STATE UNIVERSITY
SCHREYER HONORS COLLEGE

DEPARTMENT OF CHEMISTRY

FUNCTIONAL SIGNIFICANCE OF RNA SECONDARY STRUCUTRE IN AN RNA THERMOMETER FROM *BRADYRHIZOBIUM JAPONICUM*

KATHRYN BORMES
SPRING 2020

A thesis
submitted in partial fulfillment
of the requirements
for a baccalaureate degree
in Chemistry
with honors in Chemistry

Reviewed and approved* by the following:

Philip C. Bevilacqua
Distinguished Professor of Chemistry and
of Biochemistry and Molecular Biology
Thesis Supervisor

Przemyslaw Maslak
Associate Professor of Chemistry
Honors Adviser

* Electronic approvals are on file.

ABSTRACT

Through unique chemical and structural properties, mRNA is able to regulate the expression of genes via sensory RNAs within the 5' untranslated region (5' UTR). These RNAs are able to change their secondary structure when in the presence of various stimuli, such as temperature. Temperature is an important physical property highly monitored in a variety of bacteria through the expression of heat shock proteins and virulence factors. These genes are regulated through a class of noncoding temperature sensitive RNAs called RNA thermometers (RNATs). At low temperatures, the secondary structure of the RNA thermometer blocks the ribosome from binding to the 5' UTR; however, as temperature increases the RNA undergoes a conformational change that allows the ribosome to bind and initiate translation. One subclass of RNATs are ROSE (Repression Of heat Shock Expression) elements. ROSE elements are short RNA sequences that contain two to four hairpin loops and are associated with expression of small heat shock proteins. *Bradyrhizobium japonicum* is a nitrogen fixing bacteria that contains a ROSE element that encodes for a heat-shock protein. The entire 5'UTR is predicted to form three additional hairpins upstream of the RNAT. The influence of the surrounding hairpins on the RNAT are not understood. This project is aimed at determining the effect of the neighboring hairpins on the known RNAT. Through UV thermal denaturation experiments, it was concluded that the upstream hairpins do not affect the stability of the RNAT. Thus, we hypothesized that the upstream stem-loops may be necessary for proper folding of the RNAT. Using computational and experimental studies we concluded that the function of the upstream hairpins is to ensure proper folding of the RNAT.

TABLE OF CONTENTS

LIST OF FIGURES

LIST OF TABLES

ACKNOWLEDGEMENTS

I would like to express my gratitude and appreciation to Dr. Philip Bevilacqua for all the mentorship and advice he has provided me throughout this project. I am especially thankful to have been provided the opportunity as a first-year college student to pursue an independent research project and explore the joy of discovering new knowledge. I would also like to give special thanks to Dr. Elizabeth Jolley for her continuous support both in and out of lab. Her advice and guidance have proven to be a great asset within lab, the classroom, and in life. All her fun life stories and jokes will be greatly missed in addition to her endless guidance. I would lastly like to thank all past and present members of the Bevilacqua lab for welcoming me into their lab and their eagerness to assist me with any aspect of my project.

Chapter 1

Introduction to Thesis

1.1 RNA Structure and its Relation to Function

1.1.1 RNA Structure

RNA is a single-stranded nucleic acid molecule that functions in the synthesis of proteins. In contrast to DNA, RNA is single-stranded and has a hydroxyl group attached to its sugar that allows for more hydrogen bonds. These features can create complex structures through secondary and tertiary interactions. Similar to proteins, RNA primary structure is the string of nucleotides that make up the sequence. RNA secondary structure is created from intermolecular base pairing interactions within the RNA sequence that can form structures such as hairpin loops and bulges. Tertiary structure is the most advance form of structure that an RNA can form. This type of structure arises from specific interactions within an RNA strand that creates a 3-dimensional structure.

The 5' UTR nucleotide sequence upstream from the start codon can be used to regulate translation in many organisms via complex secondary structures such as riboswitches[1], small noncoding RNAs[2], and chromosomal silencing via siRNAs and micro RNAs.[3]

1.1.2 Translation Initiation within Prokaryotes

The central dogma of molecular biology is comprised of two basic processes; transcription and translation (**Figure 1.1**). Transcription is the process in which deoxyribonucleic acid (DNA) is decoded into messenger ribonucleic acid (RNA). DNA is a nucleic acid that is a double-stranded helix comprised of nucleotides and is the principle carrier of genetic material. Nucleotides are biological molecule that are comprised of a five- or six-member ring that is attached to a sugar and are the building blocks for nucleic acids. RNA is a single-stranded nucleic acid that can act as a messenger within living cells. This specific type of RNA is now as messenger (mRNA). Information encoded by DNA can be transcribed into mRNA which is then decoded by a specialized molecule called a ribosome. The ribosome then completes the second process within the central dogma of molecular biology called translation. During translation, the mRNA created during transcription is decoded by the ribosome and various other forms of RNA to create a polypeptide or protein.

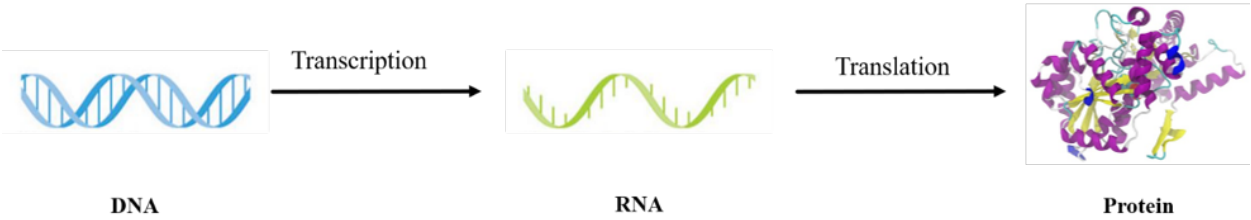

Figure 1.1 The central dogma of molecular biology. DNA is copied into RNA through a process called transcription. RNA is then decoded into a protein through a process called translation.

In some prokaryotes, the ribosome binds to the mRNA via a sequence of nucleotides called the Shine-Dalgarno (SD) sequence. Sequences of mRNA that contain a SD sequence typically have an extended 5' untranslated region (UTR) and the SD sequence is approximately 8-10 nucleotides upstream of the start codon.[4] During initiation, the small ribosome subunit (30S

in bacteria) interacts with the SD sequence via an anti-SD sequence that is complementary to the SD region within the 16S ribosomal RNA.[5,6] Through the assistance of many initiation factors, the small subunit is able to form a preinitiation complex that dissociates upon interactions with the large ribosomal subunit (50S in bacteria).[7] After the large subunit is recruited, the initiation factors dissociate and the initiating tRNA charged with N-formylmethionine aligns in the P- site, then the rest of translation is able to occur.[7] However, if the SD sequence is prevented from interacting with the anti-SD sequence translation will not occur.

1.2 RNA Thermometers

1.2.1 ROSE Elements: Structure and Function

Many genes are regulated through sensory RNAs that change complex secondary structures in the presence of various stimuli, including temperature.[8,9] Temperature is an important physical property perceived in many different types of bacteria through the expression of heat shock proteins and virulence factors.[10,11] These genes are regulated through a class of noncoding temperature-sensitive RNAs, called RNA thermometers (RNATs). At low temperatures, the secondary structure of the RNAT base pairs to the SD sequence and prevents access of the ribosome to the ribosome binding site; however, as the temperature increases, the RNA undergoes a conformational change that unpairs the SD sequence, allowing the ribosome to bind and translation to initiate.[12]

The most common RNAT is the ROSE (Repression Of heat Shock Expression) element.[13] ROSE elements are short RNA sequences that contain two to four hairpin loops and are associated with expression of small heat shock proteins (hsp).[14,15] A basic depiction of the

characteristic structure of a ROSE element is displayed in **Figure 1.2**. Within the ROSE elements, the active temperature-regulating hairpin that contains the SD sequence is the 3'-proximal hairpin (blue in **Figure 1.2**). This hairpin contains a conserved U(U/C)GCU motif that is the anti-SD sequence that base pairs to the SD region to prevent ribosome binding at low temperatures.[12,14] The central guanine (highlighted in red in **Figure 1.2**) is especially important for syn-anti base pairing with the SD sequence , and gives the RNAT its temperature sensing ability.[16]

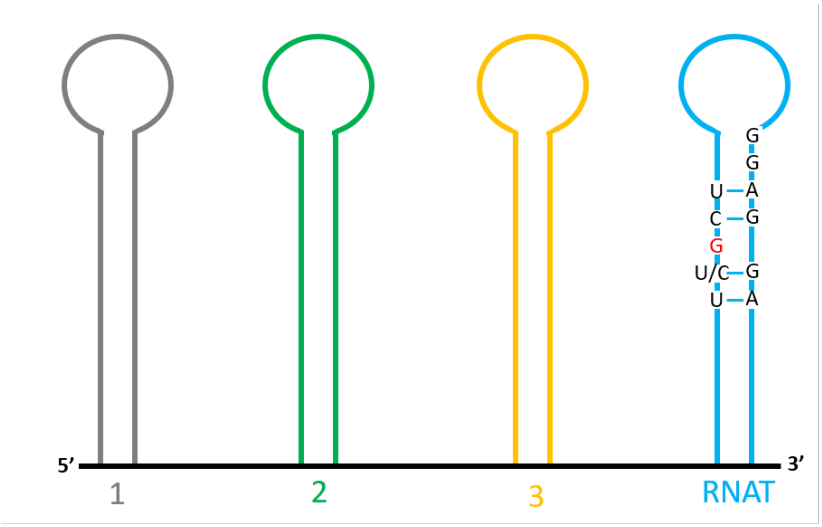

Figure 1.2 Basic structure of ROSE elements. The 3' proximal hairpin (blue) is the RNA thermometer. Within the RNAT there is the conserved U(U/C)GCU motif base pairing to the SD sequence (GGAGGA). Rose elements are characteristic of having 1-3 additional 5' upstream hairpins are illustrated as gray, green, and yellow.

1.2.2 ROSE Elements within *Bradyrhizobium japoncium*

Bradyrhizobium japonicum is a nitrogen-fixing bacterium that is known for containing multiple different ROSE elements. The 5' UTR of the ROSE element that encodes for heat shock protein A (hspA) in *B. japonicum* has an intricate secondary structure containing three hairpins

(SL1, SL2, SL3) upstream of an RNAT (**Figure 1.2**). This particular RNA structure is stabilized due to the predominantly guanine (G)-cytosine (C) base pairs (indicated by red lines in **Figure 1.2**) present within all hairpins but in higher numbers in the SL1, SL2, and SL3 hairpins. The RNAT within the ROSE element (SL4) contains more adenosine (A)-Uracil (U) base pairs and G-U wobble base pairs (Shown in **Figure 1.2** as green lines and dots, respectively) which are significantly weaker than the G-C base pairs. Since the RNAT has weaker base pairs than the other hairpins, it is predicted to be the weakest stem-loop within the entire structure.

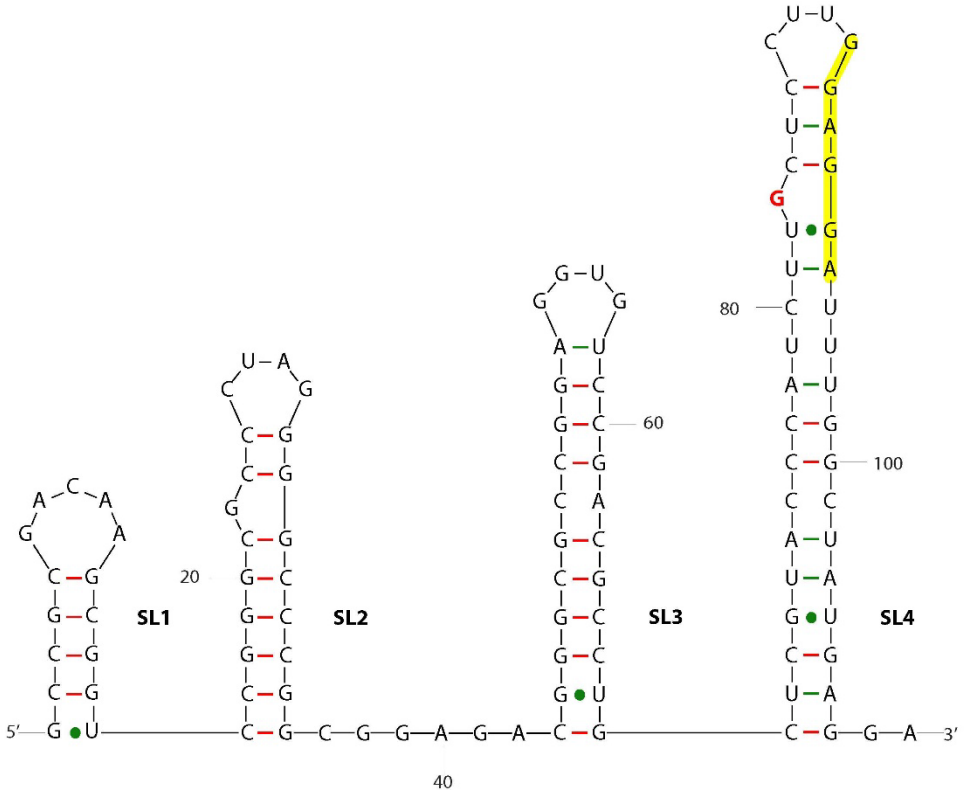

Figure 1.3 Predicted secondary structure of *B. japonicum* 5' UTR. G-C base pairs are represented by red lines, A-U base pairs are shown with green lines, and G-U base pairs are displayed as green dots. The 5' UTR is predicted to fold into four hairpins. SL4 is the previously determined RNA thermometer. The SD sequence is highlighted in yellow and the G83, which is shown in red is the conserved G residue.[16] There are three other upstream hairpins (SL1, SL2, and SL3) in addition to the RNAT. Structure prediction was created using mfold.[17]

Previously, Chowdhury et al. characterized the functionality of the 3' -proximal stem-loop (SL4) within the *B. japonicum* ROSE *in vitro* and determined the site of denaturation that

leads to the exposure of the SD sequence.[16] Furthermore, they determined that the RNAT will form a very stable hairpin that is no longer thermally labile under physiological conditions when the conserved G83 bulged residue (indicated in red in **Figure 1.2**) is deleted. These results indicate that RNATs are able to respond to fluctuations in temperatures at the level of RNA structure. Although multiple experiments were focused on the 3' proximal stem-loop, it is not clear how the upstream stem-loops contribute to the temperature-sensing function of the ROSE elements.[18]

Chapter 2

Optimization of T7 Transcription of the 5' UTR of hspA in *Bradyrhizobium japoncium*

2.1 Abstract

The RNA sequence in the 5' untranslated region (UTR) in *Bradyrhizobium japonicum* contains a higher guanine-cystosine content and the predicted folded structure has multiple stem-loop structures. The stability of this structure led to issues transcribing the DNA template of interest into the full-length UTR RNA. It is hypothesized that the stability of the 5' UTR RNA sequence and subsequently the DNA template of *B. japonicum* caused the T7 polymerase to detach from the transcript early, resulting in failed transcriptions and poor RNA yields. The final optimized transcription protocol involved a hemi-duplex transcript at physiological temperature with 20% T7 polymerase; four times the amount of polymerase typically used. The optimized protocol resulted in high RNA yields that were verified to be full length via PAGE (8% acrylamide and 8.3 M urea). The high yields were most likely due to the hemi-duplex template facilitating better attachment of the polymerase through the T7 promoter region and the excess of

T7 polymerase increasing the chances of the polymerase to attach to the DNA template. Furthermore, the buffer conditions of the reaction were optimized to lower the Tris and $MgCl_2$ levels and increase the DTT and spermidine concentrations. This may have increased yield by enhancing the polymerase ability of the T7 and preventing the reaction from prematurely aborting.

2.2 Introduction

Transcription is the process in which double stranded DNA becomes converted into single-stranded RNA. The process is similar to DNA replication. Ribonucleoside 5'-triphosphates (NTPs) are polymerized together in the 5' to 3' direction from a 3' to 5' DNA template.[19] Unlike in DNA replication, RNA polymerase does not require a primer to initiate transcription. *In vitro* transcriptions of a single transcript only requires one enzyme- RNA Polymerase. T7 RNA polymerase, originally derived from a bacteriophage in *E. coli*, is commonly used in *in vitro* transcription reactions due to its specificity for its promoters.[20] However, T7 polymerase activity is significantly reduced if there is no reducing agent involved. Therefore, most transcription protocols require the use of chemicals such as dithiothreitol (DTT).[21]

Furthermore, RNA is able to inhibit the activity of RNA polymerases and presents a problem when performing *in vitro* transcription. Spermidine is known to prevent the RNA inhibition of transcription, and is also used in many *in vitro* transcription protocols.[22] Magnesium ions are also commonly used in transcription reactions because they are able to stabilize the negatively charged backbones of the DNA and RNA molecules. Magnesium ion concentration

has also been shown to influence the specificity of T7 RNA polymerase and is therefore important to regulate for an effective *in vitro* transcription.[23] If an *in vitro* transcription is done correctly, then the released pyrophosphate groups from the NTPs will precipitate with the Mg^{2+} in the reaction mixture and the solution will turn cloudy.[24]

This project was aimed at determining the function of the upstream hairpins in the *B. japonicum* ROSE element. In order to study the unique secondary structure found in *B. japonicum*, the RNA of interest needed to be transcribed from DNA. Following the work by Chowdhury, et al., 2006, the sequence shown in **Table 2.1** was used in the transcription. This sequence, denoted at WT0, was used in the transcription trials instead of the Wild type sequence. Fortunately, the WT0 sequence did not change the overall structure of SL1, SL2, or SL4 but it did destabilize the structure of SL3.

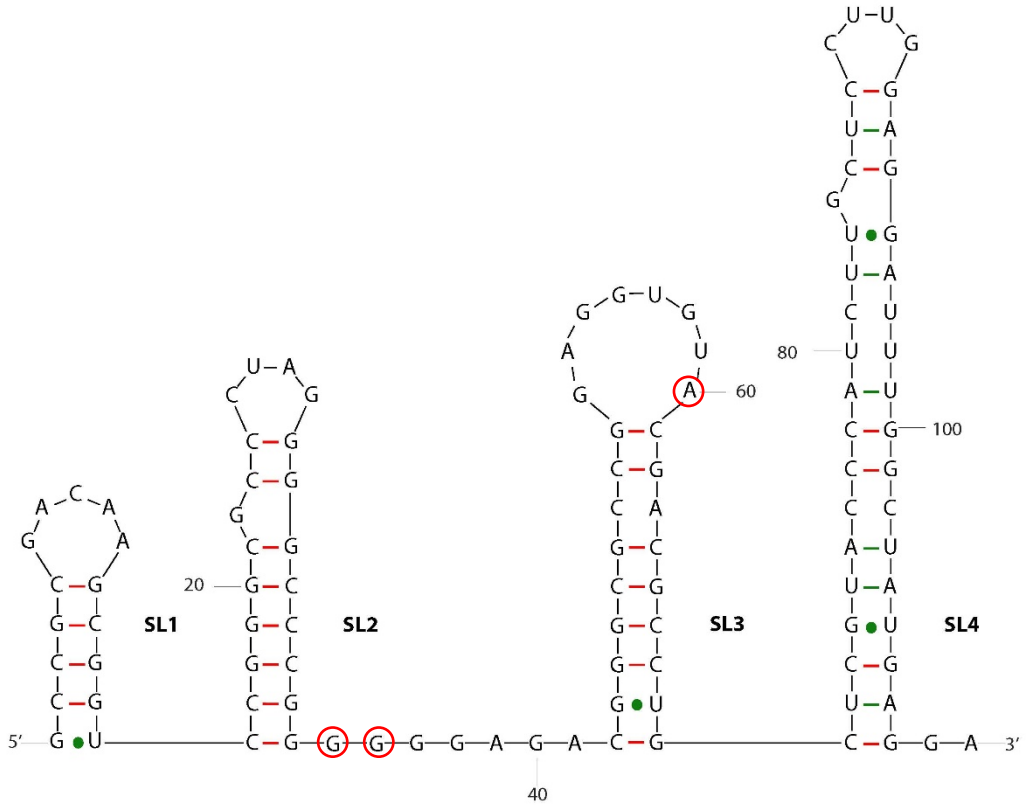

Figure 2.1 Predicted Secondary Structure of the 5' UTR of *B. japonicum* WT0 Sequence. G-C base pairs are represented by red lines, A-U base pairs are shown with green lines, and G-U base pairs are displayed as green dots. The WT0 is predicted to fold into four hairpins, with the RNAT denoted at SL4. All stem-loops except SL3 fold into the same conformation as the WT. The mutated nucleotides, circled in red, are C37G, a 38 G insert, and a C59A. Structure prediction was created using mfold.[17]

2.3 Materials and Methods

2.3.1 Original Transcription Protocol

The WT0 *B. japonicum* sequence, given below with T7 promoter region underlined, was transcribed from a gBlock® gene fragment DNA template (Integrated DNA Technologies, IDT, Coralvilla, IA) and template was used without further purification. The DNA template (100 ng/µL) and was denatured at 95 °C for 2 min in 200 mM NaCl and allowed to cool on ice for 10

min. The RNA was transcribed using 5% T7 RNA polymerase (prepared in 50% glycerol) in 40 mM Tris (pH 7.5), 2 mM DTT, 1 mM spermidine, 25 mM $MgCl_2$, and 4 mM NTPs with incubation at 37 °C for 2 h. The gBlock® gene fragment provided is double stranded, the anti-sense strand is not shown.

B. japonicum WT0 sequence DNA template of sense strand:

5' TAATACGACTCACTATAGGCCGCGACAAGCGGTCCGGGCGCCCTAGGG CCCGGGGGGAGACGGGCGCCGGAGGTGTACGACGCCTGCTCGTACCCATCTTGCTC CTTGGAGGATTTGGCTATGAGGA 3'

B. japonicum RNA Product:

5' GCCGCGACAAGCGGUCCGGGCGCCCUAGGGGCCCGGGGGGAGACGGGCG CCGGAGGUGUACGACGCCUGCUCGUACCCAUCUUGCUCCUUGGAGGAUUUGGCUA UGAGGA 3'

2.3.2 Optimized Transcription Protocol

The WT0 *B. japonicum* sequence was transcribed from a hemi-duplex template, with T7 promoter region underlined in the DNA template. The T7 promoter top strand and DNA template were ordered from IDT (Integrated DNA technologies, Coralvilla, IA) and used without further purification. The DNA template (12.5 μM) and T7 promoter (15 μM) were annealed by heating to 95 °C for 2 min in 200 mM NaCl and then allowed to cool on ice for 10 min. The DNA was transcribed using 20% T7 RNA polymerase (prepared in 50% glycerol) in 25 mM Tris (pH 7.5), 5 mM DTT, 2 mM spermidine, 20 mM $MgCl_2$, and 4 mM NTPs with incubation at 37 °C for 3 h.

T7 promoter: 5' TAATACGACTCACTATAGG 3'

B. japonicum WT0 sequence hemi-duplex DNA template:

5' TCCTCATAGCCAAATCCTCCAAGGAGCAAGATGGGTACGAGCAGGCGTC GTACACCTCCGGCGCCCGTCTCCCCCCGGGCCCCTAGGGCGCCCGGACCGCTTGTCG CGGCCCTATAGTGAGTCGTATTA 3'

B. japonicum RNA Product:

5' GCCGCGACAAGCGGUCCGGGCGCCCUAGGGGCCCGGGGGGAGACGGGCG CCGGAGGUGUACGACGCCUGCUCGUACCCAUCUUGCUCCUUGGAGGAUUUGGCUA UGAGGA 3'

2.3.3 RNA Purification

Transcribed RNA was denatured for 2 min at 95°C and purified via an 8% 8.3 M urea denaturing polyacrylamide gel. The RNA was excised from the gel and eluted in 1 X TEN_{250} (10 mM Tris at pH 7.5, 1 mM EDTA, 250 mM NaCl) at 4°C overnight while rotating. The RNA was ethanol precipitated and resuspended in 0.5X TE (10 mM Tris at pH 7.5, 1 mM EDTA). The concentration of RNA was determined using DeNovix Ds-11+ Spectrophotometer.

2.3.4 PCR Reaction

Polymerase chain reaction (PCR) was performed according to the recommended Fragment Amplification protocol for gBlocks® Gene Fragments from IDT (Integrated DNA technologies, Coralvilla, IA). In a 50 µL reaction, 1.0 ng of DNA was mixed with 1X Phusion GC Buffer, 200 µM dNTPs, 500 µM forward primer, 500 µM reverse primer, and 1% Phusion® DNA polymerase. The reaction mixture was placed in a Biometra TAdvanced Thermocycler and

amplified according to the cycling conditions details in **Table 2.1** DNA from PCR was purified using phenol/chloroform extraction followed by ethanol precipitation.

Forward Primer: 5' TAATACGACTCACTATAGGCCAC 3'

Reverse Primer: 5' TCCTCATAGCCAAATCCTCC 3'

Table 2.1 Cycling conditions for PCR.

Step	Cycle	Temperature (°C)	Time
Initial Denaturation	1	98	30 sec
Denaturation	15	98	10 sec
Annealing	15	60	30 sec
Extension	15	72	30 sec
Final Extension	1	72	5 min
Hold	1	4	∞

2.4 Results and Discussion

2.4.1 Varying Buffer Conditions

Initially, gBlocks® Gene Fragments double-stranded DNA fragments of the *B. japonicum* WT0 5' UTR containing a T7 promoter region were used in the original transcription protocol, as described in **2.3.1 Original Transcription Protocol**. When all reactions failed to work, the buffer conditions were altered so as to improve yield and optimize the reaction. **Table 2.2** outlines the different reaction conditions used throughout these trial experiments.

Table 2.2 Various buffer conditions used in transcription trials

	Tris (pH 7.5)	$MgCl_2$	DTT	Spermidine
Buffer 1	40 mM	25 mM	2 mM	1 mM
Buffer 2	25 mM	20 mM	5 mM	2 mM
Buffer 3	20 mM	25 mM	2 mM	1 mM
Buffer 4	40 mM	18.5 mM	2 mM	1 mM

All reactions using the various buffer conditions described in **Table 2.2** failed to have pyrophosphate crashing out of solution and were deemed to have failed. As a secondary check, the transcriptions were run on an 8% PAGE (8% acrylamide and 8.3 M Urea) and stained with SYBR gold but no RNA was able to be visualized.

2.4.2 Varying DNA Sequence and Deoxyoligonucleotides

Since the *B. japonicum* sequence is very rich in G-C content, another transcription was performed that increased the concentration of G and C dNTPs two-fold. Unfortunately, this still did not produce a successful transcription. Since the buffer conditions appeared to have little effect on the transcription, it was deduced that the DNA template itself may be the issue. One reason that the transcription might have failed was because of there was not enough DNA template to produce the RNA. Therefore, the DNA was amplified using PCR. The PCR products were then run on an 8% PAGE (8% acrylamide and 8.3 M Urea) and produced a transcript that was less than 100 bp. Since the full length WT0 DNA sequence is 130 bp, this sequence was

determined to be too small (**Figure 2.2**) and therefore there must have been an issue with the PCR template.

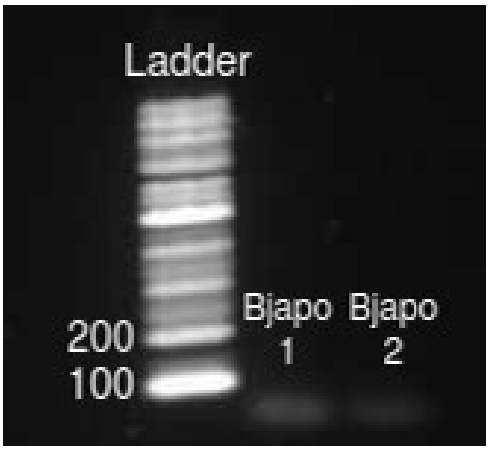

Figure 2.2 SYBR gold stained 8% PAGE (8% acrylamide and 8.3M Urea) of PCR reaction. The 100 bp ladder from New England BioLabs® was used. The *B. japonicum* WT0 DNA sequence is 110 bp; however, the band from the PCR reaction was below 100 bp.

When transcribing DNA, RNA T7 polymerase is able to protect the sequences from cleavage and hence improve the success of the reaction. The synthesis of guanine RNA nucleotides at the beginning of transcriptions has been shown to expand the length of protected DNA sequence and stabilize the polymerase-DNA interaction.[25] Therefore, a new *B. japonicum* WT0 sequence was ordered that contained GGA at the beginning of the transcript. When ran in 5% polymerase with buffer 1, 2, 3, and 4, all reactions still failed to produce any RNA.

Typically, *in vitro* transcription involves a double stranded DNA template; however, another method of transcription uses a hemi-duplex transcript, displayed in **Figure 2.3**, which contains a promoter region followed by the complement of the transcript of interest. Since T7 RNA polymerase can attach to DNA with greater success if the sequence starts with guanine bases, the T7 promoter region began with two guanine base pairs.

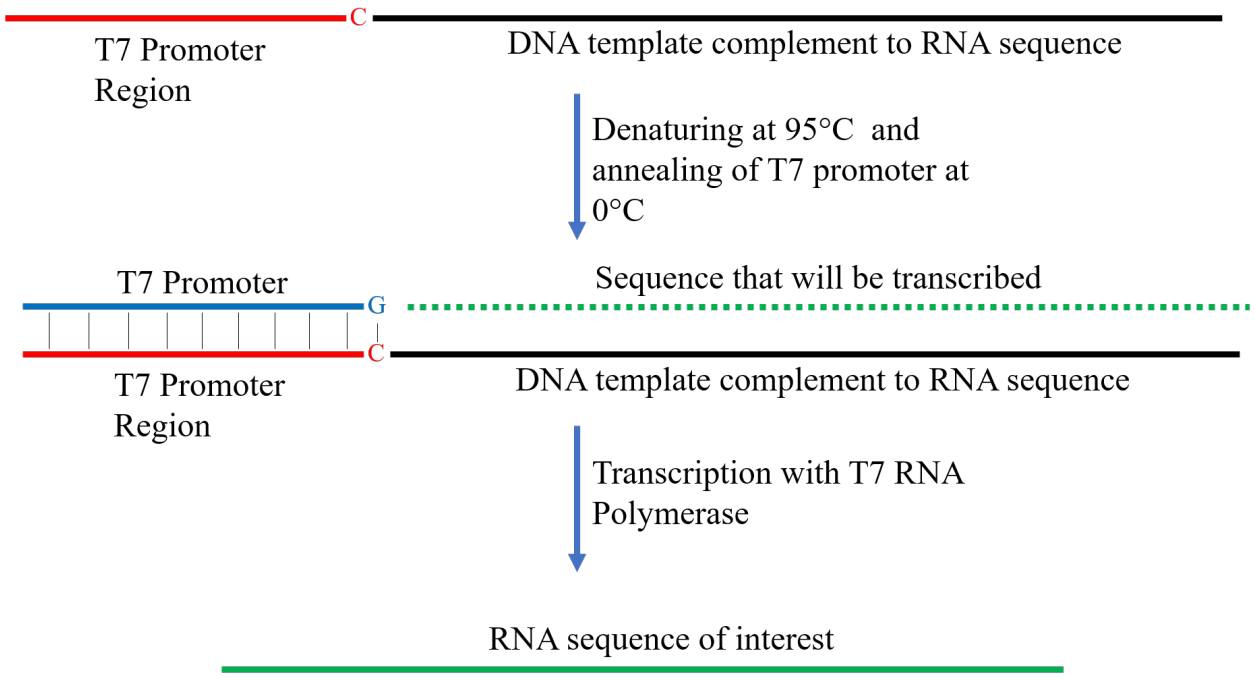

Figure 2.3 Basic overview of transcription using a hemi-duplex template

Using the hemi-duplex template at 37°C with 5% T7 polymerase in buffers 2, 3, or 4 (refer to Table 2.2), all transcriptions reactions turned cloudy and indicated that the reaction may have been successful. Typically, transcription reactions produce a few thousands of ng/ µL of RNA; however, when the RNA yields from these transcriptions were checked on a spectrophotometer, only 54.9 ng/µL, 274.1 ng/µL, 64.0 ng/µL, and 53.4 ng/µL were obtained for buffers 1, 2, 3, and 4 respectively. Furthermore, when ran on a 10% PAGE (10% acrylamide and 8.3 M Urea) and shadowed under UV light (**Figure 2.4**), there was no one clean band at the

appropriate length and it appeared that many smaller, aborted transcripts were produced instead of the desired full-length transcript.

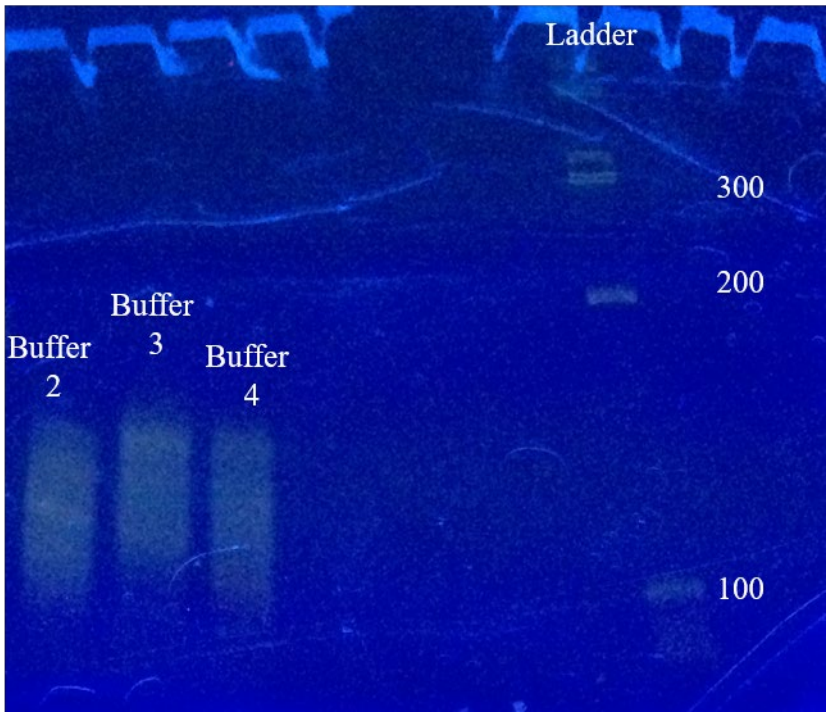

Figure 2.4 UV shadowed PAGE (10% acrylamide and 8.3 M Urea) of incomplete hemi-duplex transcription in various buffers. The Ambion® RNA Century™-Plus Marker was used as the single stranded RNA ladder. Transcriptions were performed in 37 °C with 5% T7 polymerase with a hemi-duplex template. Various buffer conditions were used and full-length transcripts were not produced. The transcription must have aborted multiple times at smaller lengths to produce a mixture of various RNA lengths.

2.4.3 Varying Reaction Conditions

Since the RNAT is predicted to form an intricate secondary structure and RNA is known to unfold at higher temperatures, we wanted to see if raising the temperature during transcription would unfold any structure and allow the T7 RNA polymerase to complete transcription. Although the transcription became cloudy, the RNA yields were only 5.7 ng/µL and 69.9 ng/µL for buffer 2 and 3, respectively, which are far too low to be fruitful.

Since the trial transcriptions produced many different terminated transcripts, there may have been an issue with the ribosome attaching to the DNA template. We therefore increased the concentration of T7 RNA polymerase in the reaction. Finally, when using 20% T7 RNA polymerase, the reactions resulted in 6090.8 ng/µL and 5620.4 ng/µL in buffers 2 and 3, respectively. In addition to producing enough RNA to be useful, a single band was produced at when run on an 8% PAGE (8% acrylamide and 8.3 M Urea) and stained with SYBR gold (**Figure 2.5**),indicating that the RNA was all the proper size and there was negligible amounts of aborted transcripts produced. Furthermore, the band was at ~110 bp which was the expected length for the WT0 sequence. Since the T7 polymerase was prepared in 50% glycerol, the total amount of glycerol in the reaction would be 10%. Since glycerol can help initiation transcription at certain promoters[26], the increase in glycerol may have also assisted in producing a successful transcription.

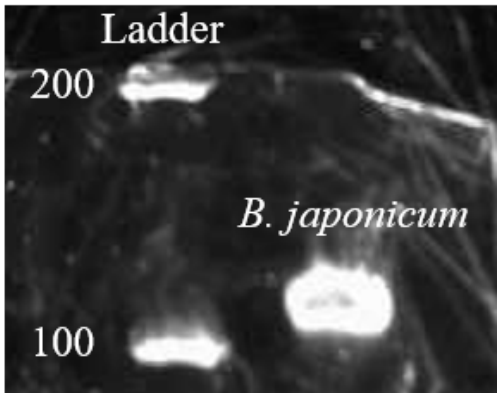

Figure 2.5 SYBR gold stained 8% PAGE (8% acrylamide and 8.3 M Urea) with *B. japonicum* mutant RNA produced from optimized transcription protocol. The Ambion® RNA Century™-Plus Marker was used as the single stranded RNA ladder. Transcription was performed at 37 °C with 20% T7 polymerase with a hemi-duplex template. Buffer 2 conditions were used and transcription produced a singular band at ~110 bp, which is the correct length for the sequence.

An overview of all the transcription conditions explored and their outcome is summarized in **Table 2.3**.

Table 2.3 Overview of transcription trials and conditions. Outcomes of each trial were judged based upon if the reaction became cloudy and was visible on a gel and then if the RNA yields were appreciable enough to be used in experimentation. The main conditions altered were the reaction buffers of the transcription, the temperature the reaction occurred at, and the amount of T7 polymerase used.

Transcript	Buffer	Temperature	T7 Polymerase	Transcription becoming cloudy and visible on PAGE (8% acrylamide and 8.3M Urea)	RNA Yields (ng/µL)
B. japonicum WT0 sequence gBlocks®	Buffer 1	37 °C	5%	X	N/A
	Buffer 2	37 °C	5%	X	N/A
	Buffer 3	37 °C	5%	X	N/A
	Buffer 4	37 °C	5%	X	N/A
B. japonicum WT0 sequence beginning with GGA gBlocks®	Buffer 1	37 °C	5%	X	N/A
	Buffer 2	37 °C	5%	X	N/A
	Buffer 3	37 °C	5%	X	N/A
	Buffer 4	37 °C	5%	X	N/A
B. japonicum WT0 sequence hemi-duplex	Buffer 1	37 °C	5%	✓	54.9
	Buffer 2	37 °C	5%	✓	274.1
	Buffer 3	37 °C	5%	✓	64.0
	Buffer 4	37 °C	5%	✓	53.4
	Buffer 2	42 °C	5%	✓	5.7
	Buffer 3	42 °C	5%	✓	69.9
	Buffer 2	37 °C	20%	✓	6090.8
	Buffer 3	37 °C	20%	✓	5620.4

Chapter 3

UV Thermal Denaturation Melts Determine that Upstream Hairpins Do Not Influence RNAT Stability

3.1 Abstract

When bacteria experience sudden increases in temperature, they produce heat shock proteins to help stabilize and prevent denaturation of their proteins. Many heat shock genes in bacteria are regulated through a class of noncoding, temperature-sensitive RNA stem-loop, called an RNA thermometer (RNAT). The most widely studied RNAT is the Repression Of heat Shock Expression (ROSE) element. ROSE elements are short RNA sequences that contain two to four stem-loop loops and are associated with expression of small heat shock proteins. Bradyrhizobium japonicum is a nitrogen-fixing bacterium that is well known for containing multiple different ROSE elements. The 5' UTR of the ROSE element that encodes for heat shock protein A (hspA) in B. japonicum has an intricate secondary structure containing three stem-loops upstream of the RNAT stem-loop. While the RNAT stem-loop within the 5'UTR of B. japonicum has been previously studied, it is not clear how the upstream stem-loops contribute to the temperature-sensing function of the ROSE elements. This relationship was studied using UV thermal denaturation in various Mg2+ buffer conditions comparing the full-length sequence to the individual stem-loops. In each Mg2+ concentration, the WT sequence showed several transitions within the melting curve indicating that the RNA sequence is not folding in a two-state manner. The melt curve experiments of the individual stem-loops revealed that the upstream stem-loops are more thermally stable than the RNAT. A construct containing the immediately upstream stem-loop and the thermometer demonstrated a similar melting curve

compared to the respective individual stem loops. Furthermore, a mutant that disrupted base pairing in the immediately upstream stem-loop of the RNAT had little direct influence on the RNAT but caused the other upstream stem-loops to melt in a two-state manner. Therefore, while the upstream stem-loops can directly influence each other melting, they do not impact the RNAT stability and may function to instead regulate its proper folding.

3.2 Introduction

More recent literature searchers revealed that the WT0 sequence that the optimization reactions were performed on deviated from the actual *B. japonicum* 5' UTR WT sequence (**Figure 1.2**). Even though the optimization reaction designed in **Chapter 2** was created using a different sequence, similar results were obtained when performed on the correct WT sequence.

Although experiments have focused on the 3' proximal stem-loop (RNAT), it is not clear how the upstream stem-loops contribute to the temperature-sensing function of the ROSE element in *B. japonicum*.[18] Since each stem-loop in the structure has varying stability, it is predicted that each individual hairpin will have distinct melting temperatures. If the upstream hairpins directly assist with the stability of the thermometer, it would be expected that the upstream hairpins melt with the RNAT in a two-state fashion. However, results from this study indicate that the full-length RNA does not melt in a two-state manner and that the upstream hairpins have an alternative function, perhaps to assist with folding or prevent misfolding.

3.3 Materials and Methods

3.3.1 RNA Preparation and Purification

When evaluating the amount of RNA necessary to complete the experiments described henceforth and the number of different templates necessary to fully investigate this system; most of the RNA sequences were ordered instead of created through a transcription reaction. The C59A Mutant, SL4, SL3, SL2, and SL1 RNA sequences were from Integrated DNA Technologies (IDT; Coralville, IA) and used without further purification.

C59A Mutant Sequence:

5’ GCCGCGACAAGCGGUCCGGGCGCCCUAGGGGCCCGGCGGAGACGGGCGC CGGAGGUGUACGACGCCUGCUCGUACCCAUCUUGCUCCUUGGAGGAUUUGGCUAU GAGGA 3’

SL1 sequence: 5’ GCCGCGACAAGCGGU 3’

SL2 sequence: 5’ CCGGGCGCCCUAGGGGCCCGG 3’

SL3 sequence: 5’ CGGGCGCCGGAGGUGUCCGACGCCUG 3’

SL4 sequence: 5’ CUCGUACCCAUCUUGCUCCUUGGAGGAUUUGGCUAUGAGGA 3’

The full-length wild type sequence and SL3-SL4 construct were prepared as complementary hemi-duplex DNA with T7 promoter region (underlined in DNA template) from IDT and used in the optimized transcription protocol outlined in **2.3.2 Optimized Transcription Protocol** and purified according to **2.3.3 RNA Purification.**

T7 promoter: 5’ TAATACGACTCACTATAG 3’

FL WT *B. japoncium* sequence DNA template:

5’ TCCTCATAGCCAAATCCTCCAAGGAGCAAGATGGGTACGAGCAGGCGTC GGACACCTCCGGCGCCCGTCTCCGCCGGGCCCCTAGGGCGCCCGGACCGCTTGTCGC GGCCCTATAGTGAGTCGTATTA 3’

FL WT *B. japoncium* sequence:

5’ GCCGCGACAAGCGGUCCGGGCGCCCUAGGGGCCCGGCGGAGACGGGCGC CGGAGGUGUCCGACGCCUGCUCGUACCCAUCUUGCUCCUUGGAGGAUUUGGCUAU GAGGA 3’

SL3-SL4 *B. japoncium* construct DNA template:

5’ TCCTCATAGCCAAATCCTCCAAGGAGCAAGATGGGTACGAGCAGGCGTC GGACACCTCCGGCGCCCGCCTATAGTGAGTCGTATTA 3’

SL3-SL4 *B. japoncium* construct sequence:

5’ CGGGCGCCGGAGGUGUCCGACGCCUGCUCGUACCCAUCUUGCUCCUUGG AGGAUUUGGCUAUGAGGA 3’

3.3.2 UV Thermal Denaturation Melts

RNA was added to 100 mM KCl and 100 mM HEPES at pH 7.0. The RNA was then denatured at 95°C for 3 min and cooled at room temperature for 10 min. Appropriate concentrations of $MgCl_2$ (0 mM, 0.5 mM, or 2 mM) was added to the RNA solution and incubated at 55°C for 3 min and cooled at room temperature for 10 min. The thermal denaturation experiments were performed on the OLIS Hewlett Packard 8452A Diode Array Spectrophotometer. Data points were collected every 0.5°C at a heating rate of ~0.6°C/min. Absorbance was recorded at 260 nm and the first derivative of each curve was obtained by

smoothing the raw absorbance values of a representative data set with an 11-point window. Normalized graphs are found in Appendix A. Estimated melting temperatures (T_m) were determined from the local maximum of the first derivative plot.

3.3.3 Simulated UV Thermal Denaturation Melt Curves

Equations used to simulate the melt curves are described in Appendix B. The percent of RNA folded was determined for a range of temperatures. Thermodynamic properties used in these equations were obtained from mfold RNA Folding Form (version 2.3 energies).[17] The simulated RNA was folded at 37°C in 1 M NaCl with no divalent ions.

3.3.4 Concentration-Dependent UV Thermal Denaturation Melts

Melts were performed according to the UV Thermal Denaturation Melt protocol described in **3.3.2 UV Thermal Denaturation Melts** with the exception that 0.5 mM $MgCl_2$ was used for all melts and the RNA concentration varied as follows: 0.5 μM, 1 μM, 2 μM, 3.5 μM, and 5 μM RNA. The concentration of RNA in each sample was verified by a Beers Law calculation using the 260 nm absorbance at 90°C.

3.4 Results and Discussion

3.4.1 Wild-Type Sequence Exhibits Multi-State Folding

In order to determine the strength of the RNA structure formed when all stem-loops are present, UV thermal denaturation melts were performed on the full-length RNA. Varying concentrations of $MgCl_2$ were used to determine the stability of the RNA since divalent cations, like Mg^{2+}, are essential for stability of the anionic nature of RNA molecules. Although monovalent cations such as K^+ are able to stabilize RNA molecules as well, they are not nearly as effective at promoting proper folding as Mg^{2+}. Since KCl has a small impact on folding, the concentration of KCl remained constant throughout the experiments. The biological concentration of KCl ranges from 100-150 mM[27]; therefore, 100 mM of KCl was used to replicate the conditions used by Chowdhury et al.[16] Furthermore, the biological concentration of Mg^{2+} in prokaryotic cells is 1.5-2.0 mM[28,29] and 0.5-1.0 mM in eukaryotic cells.[30] Therefore, melts performed in 2 mM $MgCl_2$ mimicked prokaryotic cells and 0.5 mM $MgCl_2$ represented eukaryotic cells conditions.

In each Mg^{2+} concentration, the WT sequence displayed several transitions (**Figure 3.1**). Each curve had a clear transition ranging between 50-65°C, with another transition starting around 95°C. Since Mg^{2+} is important for stabilizing the RNA native structure, it was not surprising that the T_m increased with $MgCl_2$ concentration: 50.3°C, 62.3°C, and 63.8°C in 0 mM, 0.5 mM, and 2 mM $MgCl_2$, respectively. The multiple transitions within the melting curve indicate that the RNA sequence is not melting in a two-state fashion.

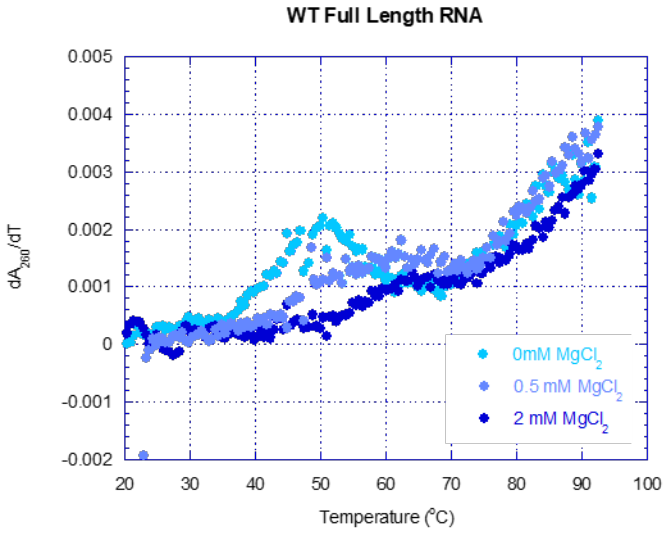

Figure 3.1 UV thermal denaturation first derivative curves of the WT RNA in *B. japonicum.* Absorbances were measured at 260 nm in 0 mM, 0.5 mM, and 2 mM $MgCl_2$ (light to dark colors). The T_m values were 50.3°C, 62.3°C, and 63.8°C in 0 mM, 0.5 mM, and 2 mM $MgCl_2$, respectively. Solutions contained 100 mM HEPES (pH 7.0) and 10 mM KCl.

Past studies have shown that tRNA will have an approximately two-state concerted melting transition at high Mg^{2+} concentrations, despite being comprised of four helices. This is because the stability of the tertiary structure overshadowing the stability of the individual stem-loops.[31] Lack of such a single two-state transition at all Mg^{2+} concentrations, indicate it is unlikely that the *B. japonicum* WT RNA is forming a tertiary structure.

3.4.2 Upstream Hairpins are Important for Proper Folding of the RNAT

In an attempt to assign transitions to individual stem-loops within the full-length sequence, melts were performed on the individual stem loops (represented as SL4, SL3, SL2, and SL1). Again, since Mg^{2+} stabilizes RNA, it was expected that the melting temperature of the RNA would increase with Mg^{2+} concentration. This trend was observed in the thermometer (SL4) stem-loop only, where the RNA became increasingly stable as evidenced by an increase in the T_m from 50.9°C, 57.8°C, and 58.9°C in 0mM, 0.5 mM, and 2 mM $MgCl_2$, respectively. Therefore, the transition in the WT sequence between 50-65°C in all $MgCl_2$ concentrations can be attributed to the SL4 stem-loop. In fact, the SL4 stem-loop was the only stem-loop to have a clear transition, around 50-60°C, within the temperature constraints of the instrument (**Figure 3.2**) The SL3, SL2, and SL1 display no melting transitions between 20-95°C for 0-2 mM $MgCl_2$, but appear to have an initial transition towards the upper limits of the melting range. This result was expected since the upstream stem-loops have significantly more guanine-cysteine base pairs compared to the SL4.

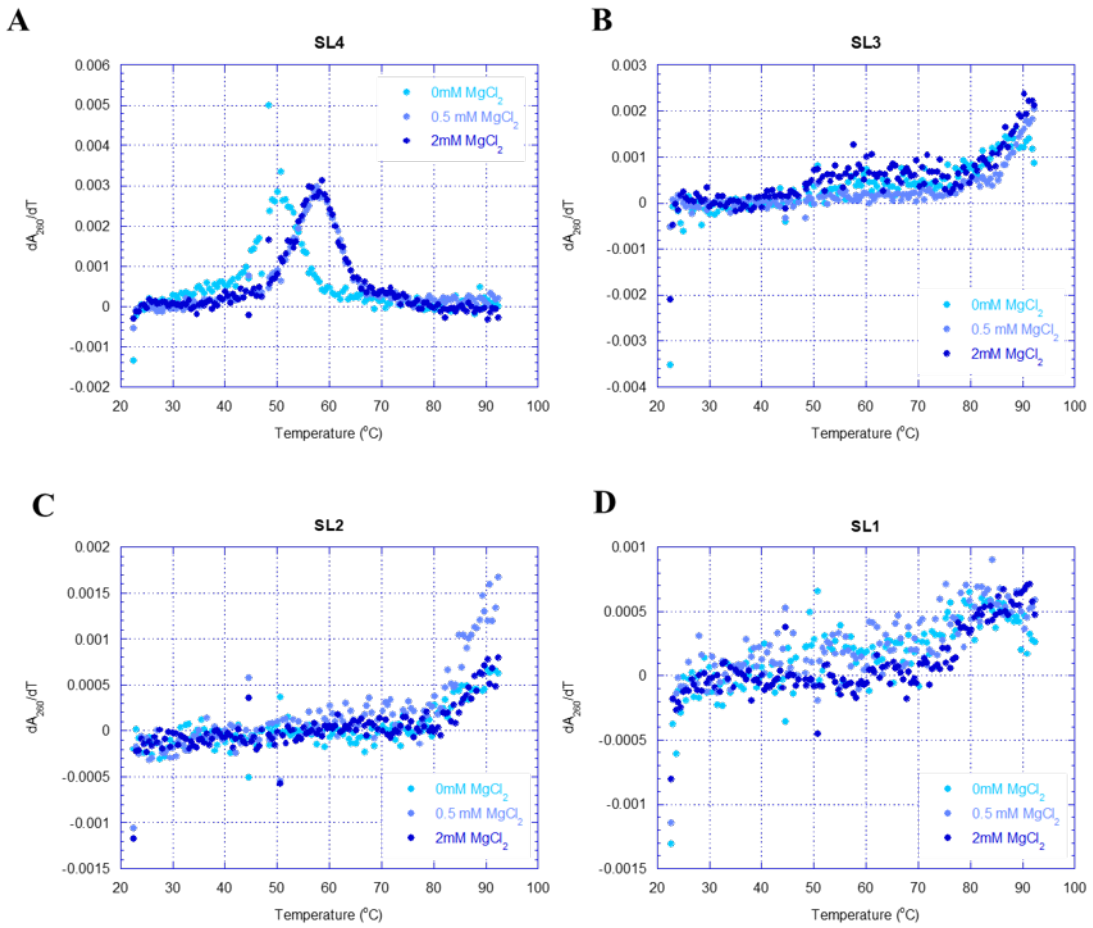

Figure 3.2 UV thermal denaturation first derivative curves of the individual stem-loops in *B. japonicum*. Absorbances were measured at 260 nm with absorbance at 280 nm is located in Appendix B. First derivative curves of the thermal denaturation experiments for A) SL4, B) SL3, C) SL2, and D) SL1 in *B. japonicum* ROSE element within 0 mM, 0.5 mM, and 2 mM $MgCl_2$ (light to dark colors). The T_m values for SL4 were 50.9°C, 57.8°C, and 58.9°C in 0mM, 0.5 mM, and 2 mM $MgCl_2$, respectively. No T_m values from SL1, SL2, or SL3 were able to be determined. Solutions contained 100 mM HEPES (pH 7.0) and 10 mM KCl.

To verify if the experimental data indicated that the stem-loops were melting in a two-state model, the melt curves were simulated using thermodynamic properties of each individual stem-loop (**Figure 3.3A**). According to the simulations, the T_m values are 93.2°C, 86.1°C, 94.1°C, 70°C for SL1, SL2, SL3, and SL4, respectively (**Figure 3.3B**). The predicted T_m values were not

an accurate reflection for the experimentally derived values for SL4, and the model predicted melting temperatures which were not obtained for SL1, SL2, or SL3. However, with the exception of SL2, it appears that the melt simulation is able to prediction the general trend in melting temperature compared to the other stem-loops, which clearly predicted the completed melting of SL4 and incomplete melting of SL1 and SL3 at 95ºC. Therefore, it appears that the stem-loops are not melting in a two-state fashion and the simulation must be altered to account for intermediate structures in melting in order to be an adequate system to predict the melting of these RNA structures.

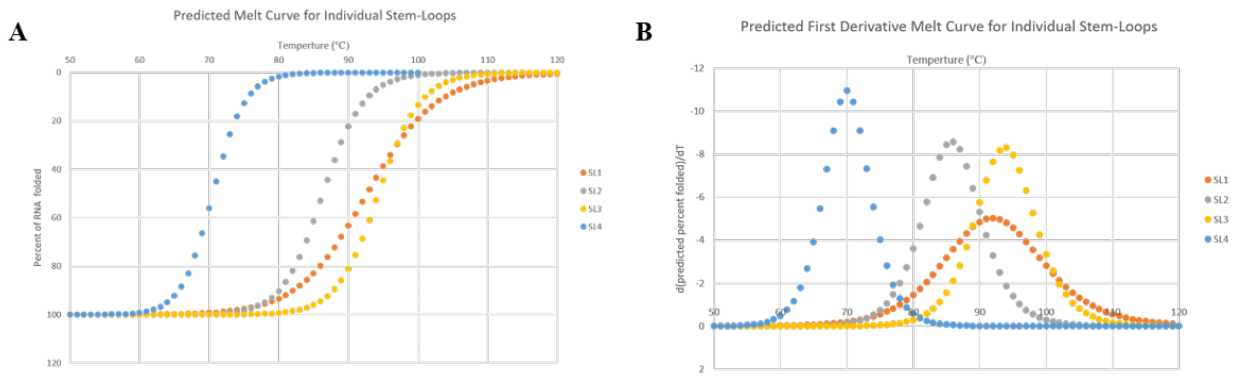

Figure 3.3 Simulated UV thermal denaturation melt curves of individual stem-loops. A) Simulated melting curves for the individual stem-loops. B) First derivative of simulated melt curve for individual stem-loops. The predicted T_m values are 93.2°C, 86.1°C, 94.1°C, 70°C for SL1, SL2, SL3, and SL4, respectively. Melt curves were simulated from thermodynamic obtained from mfold RNA Folding Form (version 2.3 energies)[17] in 1M NaCl and 0 mM $MgCl_2$. Equations used to create simulation can be found in Appendix C.

3.4.3 RNA Sequences are Not Forming Dimers During Renaturation Step

Because the RNA is forming structures through internal base pairing, there is a possibility that the RNA could dimerize during the renaturation step prior to melting. To determine if the RNA was forming dimers, melts were performed with each stem-loop using 0.5 mM $MgCl_2$ over

a 10-fold range of RNA concentrations (**Figure 3.4**). The 0.5 mM concentration was chosen so that there would still be a measurable T_m but it would produce a lower T_m then the 2 mM concentration. At higher concentrations of RNA, it is expected that dimers would form more readily. Therefore, if the sequences were forming dimers, it would be expected that the melt curves would look different and the T_m values would vary as the RNA concentration changed. Since all the melts had similar T_m values and at the varying concentrations, it was concluded that the RNA sequences were unlikely to be forming dimers and that the melt data were an accurate reflection of the unfolding of the RNA stem-loops being studied.

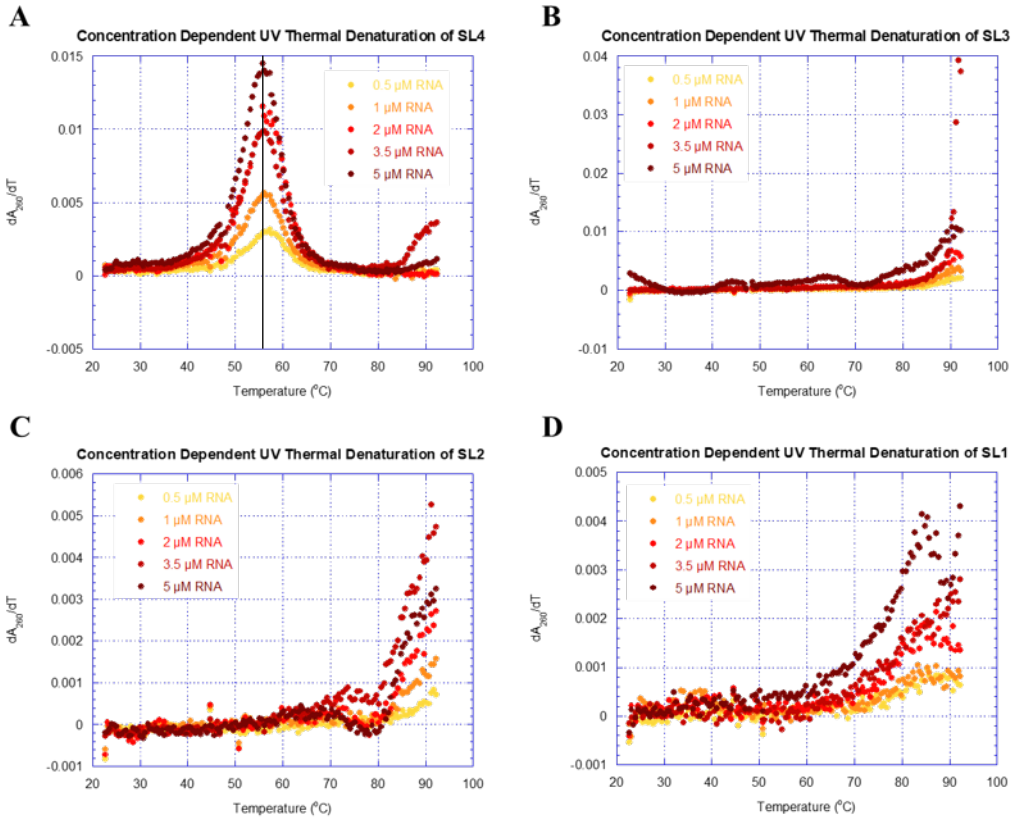

Figure 3.4 Concentration dependent UV thermal denaturation first derivative curves of the individual stem-loops in *B. japonicum.* Absorbances were measured at 260 nm for A) SL4, B) SL3, C) SL2, and D) SL1 in 0.5 mM $MgCl_2$. The melts were performed in 0.5 µM, 1 µM, 2 µM, 3.5 µM, and 5 µM RNA (light to dark colors). The T_m value for SL4 were at 55.7°C. No T_m

values from SL1, SL2, or SL3 were able to be determined. Solutions contained 100 mM HEPES (pH 7.0) and 10 mM KCl.

3.4.4 Immediately Upstream Hairpin is not Pairing with RNAT

Based on the melt curves for the individual stem loops, it is evident that the upstream stem-loops are significantly more stable than SL4. To help assess if a single stem-loop, rather than three stem-loops, could ensure proper folding of SL4, a SL3-SL4 fusion construct was made. Following the previous melt conditions, the construct was melted in varying Mg^{2+} concentration (**Figure 3.5**). Similar to the SL4 stem-loop, the construct became more thermally stable with increasing $MgCl_2$ concentration, with T_m at 48.7°C, 54.9°C, and 59.8°C at 0 mM, 0.5 mM and 2 mM $MgCl_2$ concentration, respectively. Interestingly, the construct also had the beginning of another transition at the limits of the instrument, similar to what was observed in the SL3 stem-loop. Since the melting of the construct mimicked the melting of the individual SL4 and SL3 stem-loops combined, it was concluded that only the immediately upstream stem-loop is necessary to ensure proper folding of SL4 and that SL3 does not interact or pair with the RNAT sequence.

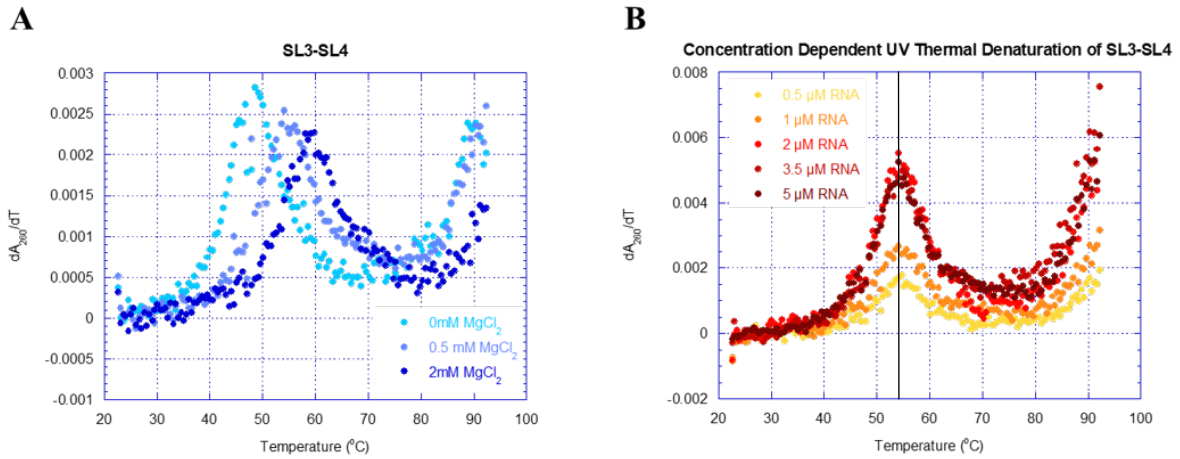

Figure 3.5 UV thermal denaturation first derivative curves for *B. japonicum* SL3-SL4 construct. A) UV thermal denaturation first derivative curves measured at 260 nm in 0 mM, 0.5 mM, and 2 mM $MgCl_2$ (light to dark colors). The T_m values were 48.7°C, 54.9°C, and 59.8°C in 0mM, 0.5 mM, and 2 mM $MgCl_2$, respectively. B) Concentration dependent UV thermal denaturation first derivative curves measured at 260 nm. The melts were performed in 0.5 µM, 1 µM, 2 µM, 3.5 µM, and 5 µM RNA (light to dark colors). The T_m value was 54.3°C. Solutions contained 100 mM HEPES (pH 7.0) and 10 mM KCl.

3.4.5 Disrupting Base-Pairing in SL3 Interferes with Melting of Upstream Hairpins Only

The increased stability of the other stem-loops could be related to their potential function in regulating the melting of SL4. To test this hypothesis, a C59A mutant of the full-length *B. japonicum* ROSE element was created that extended the unpaired loop from four to eight nucleotides within SL3 but still maintained proper folding of the other stem-loops (**Figure 3.6**).

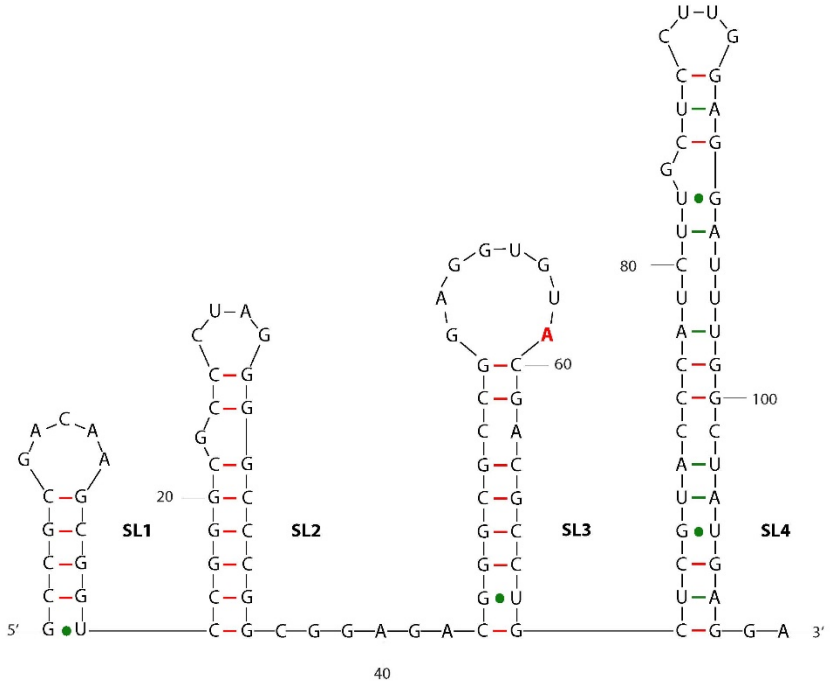

Figure 3.6 Predicted secondary structure of the 5' UTR of interest in the C59A *B. japonicum* mutant. The 5' UTR is predicted to fold into four hairpins. All stem-loops except SL3 fold into the same conformation as the WT. The mutated nucleotide in SL3 is highlighted in red and causes an additional 4 nucleotide expansion in the hairpin loop. Structure prediction was created using mfold.[17]

When melted in the same conditions as the WT sequence, the C59A mutant maintained the same melting transition near 50-60°C and a high temperature transition with increased concentrations of Mg^{2+} (**Figure 3.7**); supporting that the mutant lacks any tertiary structure. A summary of the predicted free energy, predicted values of T_m, G/C content, and measured values of T_m for all stem-loops are constructs created in this work are described in **Table 3.1**. Also similar to the WT, C59A has a prominent transition from 50-60°C that becomes more stable as the Mg^{2+} concentration increases (T_m values at 48.7°C, 55.2°C, and 59.3°C at 0 mM, 0.5 mM and 2 mM $MgCl_2$ concentration, respectively). Since this transition mimicked the transition observed from SL4, it appears that decreasing the thermal stability of SL3 does not directly

influence the melting of the RNAT. Interestingly, the C59A sequence lacked the beginning of another transition at the upper limits of the machine, which was observed in the WT and individual stem loops melts. Furthermore, there was another prominent transition in the C59A melt that can be attributed to SL1, SL2, and SL3 with T_m values at 79.3°C, 80.8°C, and 83.3°C in the 0 mM, 0.5 mM and 2 mM $MgCl_2$ concentration, respectively. Based upon these observations, decreased stability in the immediate upstream stem-loop has little effect on the melting of the RNAT, but influences the melting of the upstream stem-loops. It is likely that when SL3 is mutated to become less stable, only SL3 melts at ~70-80°C, and SL1 and SL2 are no longer melting.

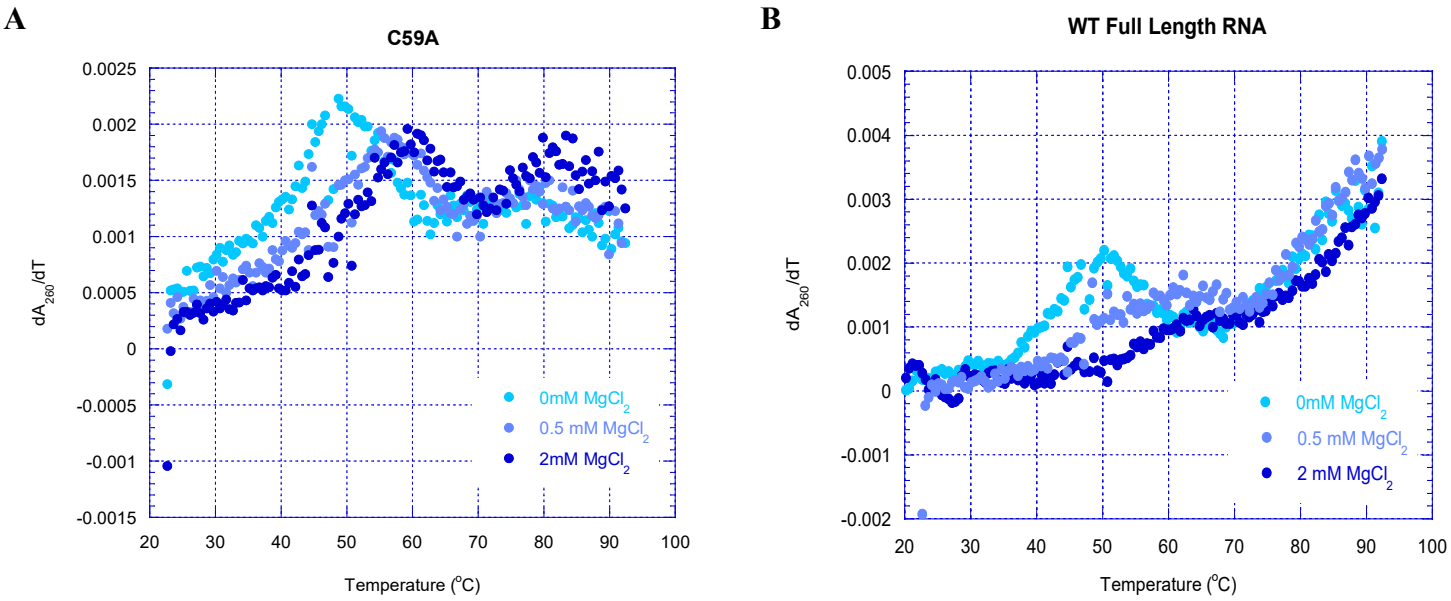

Figure 3.7 UV thermal denaturation first derivative curves of C59A *B. japonicum* mutant. The absorbance was measured at 260 nm in 0 mM, 0.5 mM, and 2 mM $MgCl_2$ (light to dark colors). A) First derivative curve for the C59A mutant. The T_m values were 48.7°C and 79.3°C, 55.2°C and 80.8°C, and 59.3°C and 83.3°C in 0 mM, 0.5 mM, and 2 mM $MgCl_2$, respectively. B) First derivative curve for the WT sequence. The T_m values were 50.3°C, 62.3°C, and 63.8°C in 0 mM, 0.5 mM, and 2 mM $MgCl_2$, respectively. Solutions contained 10 mM HEPES (pH 7.0) and 10 mM KCl.

Table 3.1 Summary of predicted and measured thermodynamic properties for all RNA sequences tested within this experiment. The predicted thermodynamic properties were obtained from mfold RNA Folding Form (version 2.3 energies) [17] at 37°C in 1M NaCl and 0 mM $MgCl_2$. Predicted T_m values were made assuming a two-state model. The measured T_m values were derived experimentally from the first derivative UV thermal denaturation melts.

RNA Sequence	Predicted ΔG (kcal/mol)	Predicted T_m (°C)	Percent G/C (%)	Measured T_m in 0 mM $MgCl_2$ (°C)	Measured T_m in 0.5 mM $MgCl_2$ (°C)	Measured T_m in 2 mM $MgCl_2$ (°C)
WT	-46.70	86.3	69.7	50.3	62.3	63.8
SL1	-8.1	92.3	73.3	N/A	N/A	N/A
SL2	-12.1	86.1	90.5	N/A	N/A	N/A
SL3	-13.9	94.1	80.8	N/A	N/A	N/A
SL4	-10	70.3	51.3	50.9	57.8	58.9
SL3-SL4 Construct	-24.5	82.4	63.1	48.7	54.9	59.8
C59A Mutant	-42.6	85.5	68.8	48.7, 79.3	55.2, 80.8	59.3, 83.3

Chapter 4

Computational Analysis of RNA Thermometer Folding Patterns

4.1 Abstract

Repression of heat shock expression (ROSE) elements are RNA Thermometers (RNAT) that are characteristic of have multiple hairpins upstream of the RNAT itself. Current work on the ROSE element in *Bradyrhizobium japonicum* is hinting to the idea that the upstream hairpins do not assist with the melting of the RNAT. Therefore, it is hypothesized that the upstream hairpins may promote proper folding of the RNAT. To test this theory, a literature search was first performed and it was determined that the upstream hairpin stability may be evolutionarily conserved. Furthermore, predictions of the secondary structure formed by the untranslated region of the ROSE element in *B. japonicum* were made. Multiple randomizations were performed that altered specific segments of the wild-type *B. japonicum* sequence. From these studies, it appears that the upstream hairpins are specifically designed to be extremely stable in order to prevent misfolding of the RNAT with the spacer sequence between SL2 and SL3 particularly vital to maintaining the integrity of SL4.

4.2 Introduction

RNA thermometers (RNATs) are temperature sensing RNA sequences that prevent translation of heat or cold shock proteins under normal physiological temperatures. One class of RNATs are repression of heat shock expression (ROSE) elements, which are known to have

multiple 5' upstream hairpins in addition to the thermometer. The function of these upstream hairpins is thus far unknown and is being explored in this study through the ROSE element found in *Bradyrhizobium japonicum.* As discussed in **Chapter 3**, the ROSE element in *B. japonicum* does not fold in a two-state manner and it was concluded that the upstream hairpins do not influence the RNAT stability. However, they may be necessary for the proper folding of the RNAT.

To assess this question, it was necessary to predict the secondary structure formed by variations of the 5' untranslated region (UTR) in *B. japonicum* using the structure prediction software, mfold.[17] This software is able to predict the most energetically favorable secondary structure for any given RNA sequence. The program is an accumulation of multiple packages that incorporate RNA folding parameters and free energy predictors. Using algorithms to predict the minimum free energy for base pairing, the program is able to produce the energetically favorable secondary structure for any given RNA input, as well as the energy parameters associated with it (free energy, melting temperatures, enthalpy, and entropy).

Using this program, different sequence randomizations of the 5' UTR in *B. japonicum* were folded and the structures predicted. Each sequence was then analyzed to determine if the RNAT would still fold into its characteristic hairpin. The results from the folding indicate that the spacer sequence between SL2 and SL3 may be especially important in regulating how the RNAT folds. In fact, most randomizations that did not result in the correctly folded RNAT were due to the wild-type (WT) spacer sequence forming base pairs within the first ten 5' nucleotides in the SL4 sequence.

4.3 Materials and Methods

4.3.1 Predicting T_m values of hairpins within other ROSE Elements

ROSE element sequences for other organisms were found via a literature search. These sequences were then segmented into the individual hairpin sequences and their structures were predicted using mfold RNA Folding Form (version 2.3 energies).[17] The most energetically favorable structure was matched to the predicted full length sequence to ensure that the hairpin still formed the same secondary structure. The predicted melting temperature (T_m) for this structure was selected. A similar approach was taken for the remaining hairpins within each ROSE element.

4.3.2 Folding of RNAT

All structure predictions were made using mfold software.[17] The predication with the most favorable free energy, ΔG, was chosen as the predominant structure formed. The 41-nucleotide sequence of SL4 was spilt into four groups of ten nucleotides with the last group containing 11 nucleotides. These groups were then added consecutively together and their structure was predicted. Since no structure was predicted for the first ten nucleotides (1/4 SL4), the next ten nucleotides were added and the structure predicted (½ SL4). The same procedure was done for the other groups of SL4 to create ¾ SL4 and the full SL4. A similar approach was taken for SL1-SL3 with the group additions occurring at the 3' end of the sequence.

4.3.3 Randomizations

Specific segments of RNA were randomized using a random RNA nucleotide generator program. These random sequences were then added to the appropriate place within the WT sequence and then entered into the mfold software.[17] The predication with the most favorable ΔG was chosen as the predominant structure formed.

4.4 Results and Discussion

4.4.1 Stability of Upstream Hairpins May be Evolutionarily Conserved

A literature search was performed to determine if highly structed 5' upstream hairpins compared to the 3' proximal RNAT is a trend within ROSE elements. Thus far only data on a few known ROSE elements found in mesophilic bacteria were analysis using predicated secondary structures and T_m (**Figure 4.1**). Thus far, there appears to be a general trend of more thermally stable upstream hairpin structures than the SD sequence containing hairpin within ROSE elements. Furthermore, in the cases observed at this point, it appears that the hairpin most directly upstream the RNAT is the most structured hairpin within the whole structure. Based upon the initial results, it appears as if the increased thermal stability of the upstream hairpins compared to the 3' proximal hairpin is trend that may be characteristic of ROSE elements and not just the ROSE element with *B. japoncium*.

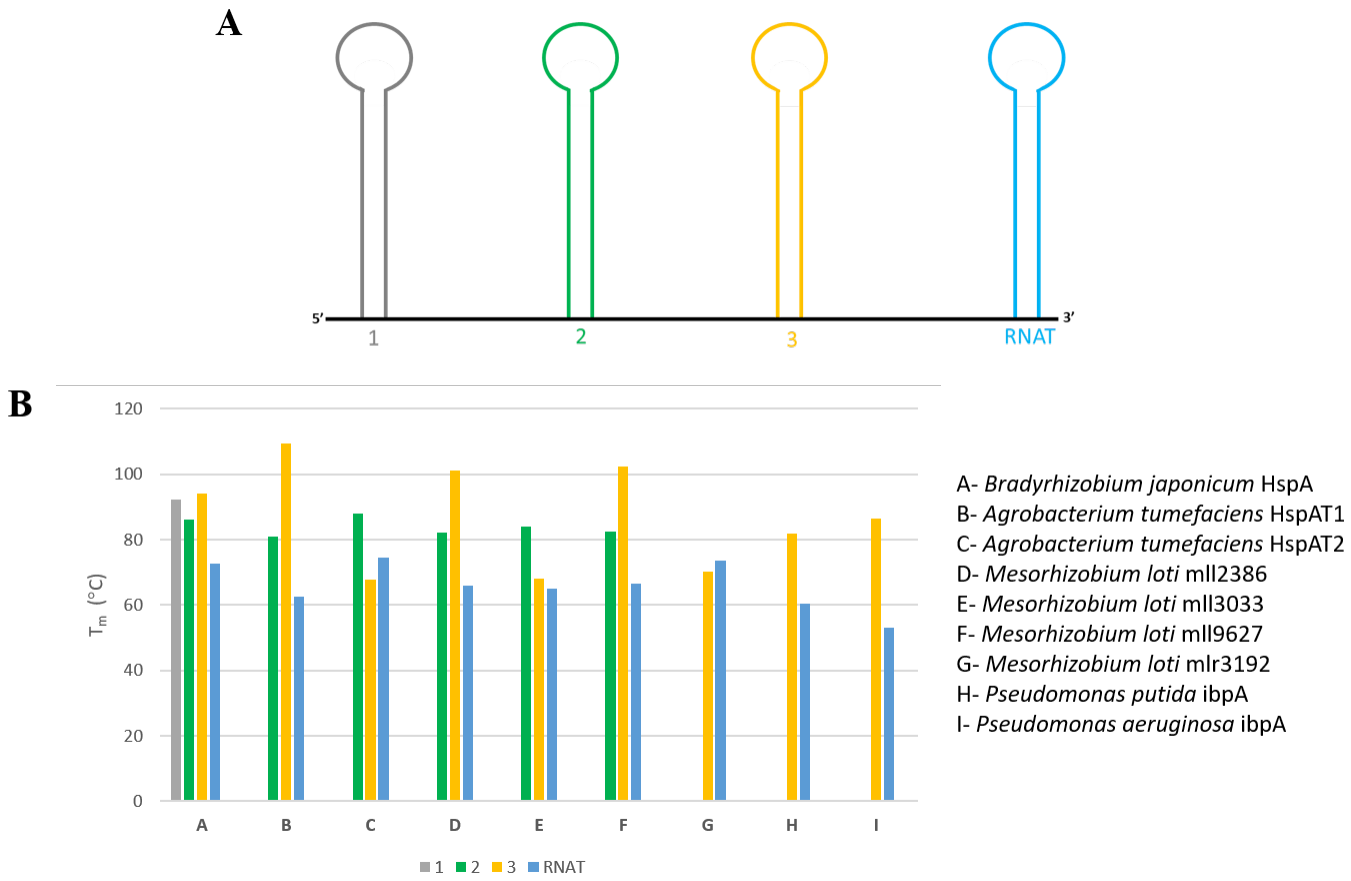

Figure 4.1 Predicted T_m for each individual stem-loop within several known ROSE elements. A) Graphic depiction of basic structure of a ROSE element. Colors depicted in panel A correspond to the bar graph legend in panel B. B) Organism and gene name for each ROSE element are described in the legend to the right. Each RNA sequence was analyzed using mfold RNA Folding Form (version 2.3 energies) to determine the most stable predicted secondary structure and calculate an appropriate T_m. [17]

4.4.2 RNAT Folding Changes in the Presence of Upstream Hairpins

UV thermal denaturation experiments suggest that the upstream hairpins (SL1-SL3) do not directly influence the melting of the RNAT (SL4), so it was hypothesized that they may function to ensure proper folding. Structures with various lengths of SL4 with and without the upstream hairpins were created (**Figure 4.2**). When the sequence for ½ SL4 is folded (4.2A), it

begins to form a small hairpin that is not observed for ¾ SL4 or SL4 (4.2B-4.2C). Interestingly, this smaller hairpin formed with only ½ SL4 and is never formed when ½ and ¾ SL4 is folded with the addition of the upstream sequence for SL1, SL2, and SL3(4.2D-4.2E). In fact, this hairpin is prevented from folding due to additional base-pairing between the first three nucleotides of SL4 with the last three nucleotides of the 6 nucleotide non-base-paired spacer sequence between SL2 and SL3. This base-pairing is not disrupted until the full SL4 is folded with SL1-SL3 (4.2F). Therefore, it appears that SL3 may prevent misfolding of SL4. This could have important biological function as the immediate upstream hairpin may tie up the RNAT sequence while during transcription.

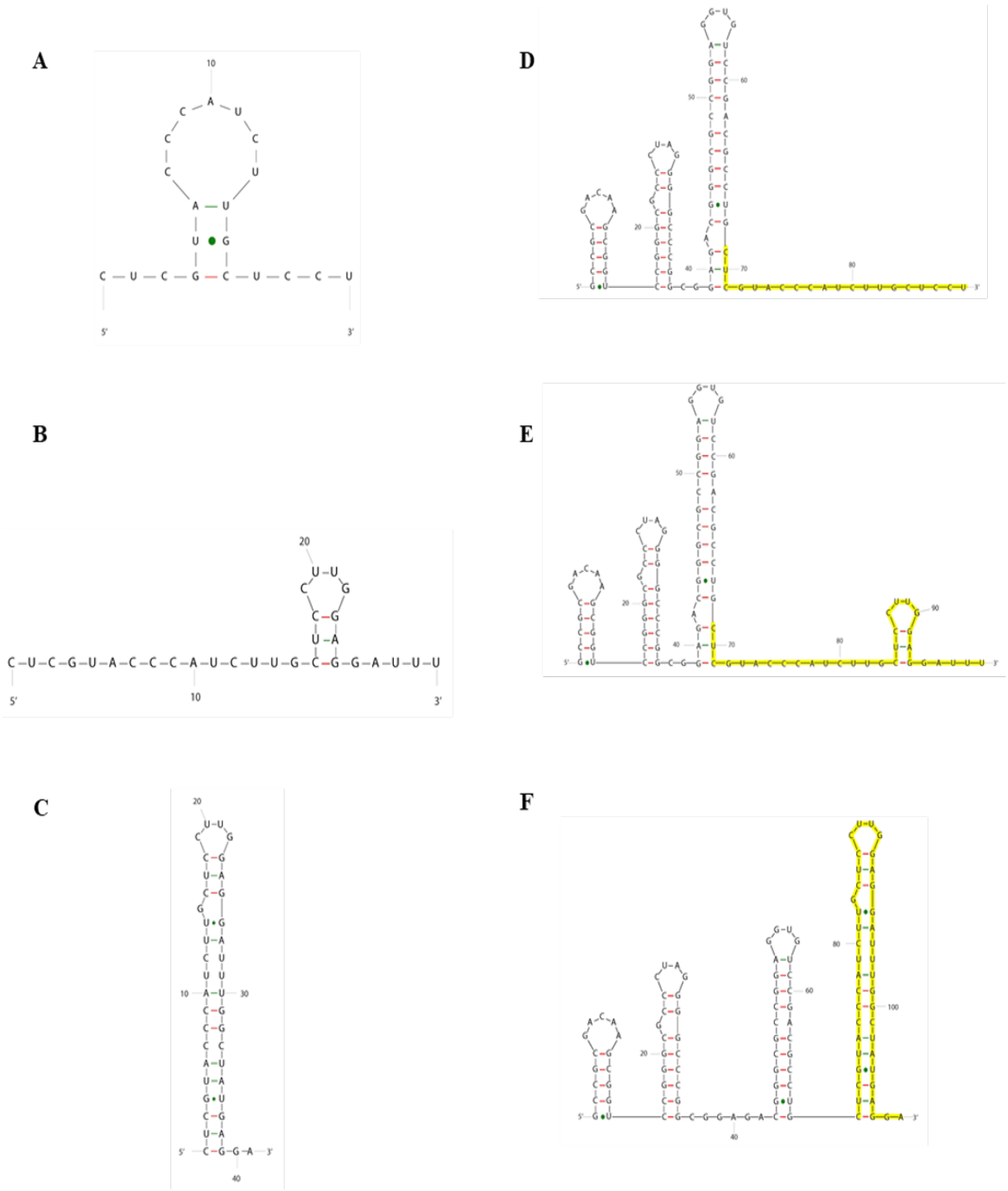

Figure 4.2 Secondary structure predictions of various lengths of RNAT with and without upstream hairpins. The secondary structure predictions were prepared using mfold[17] for A) ½ SL4, B) ¾ SL4, C) SL4 D) SL1-SL3 and ½ SL4, E) SL1-SL3 and ¾ SL4, F) Full length sequence of 5' UTR of interest in *B. japonicum.* The added SL4 sequence is highlighted in yellow.

4.4.3 Structural Predications Indicate that Spacer Between SL2 and SL3 May Ensure Proper Folding of RNAT

Since it appeared that folding is assisted mainly through SL3, we wanted to determine if that sequence was specific to forming the RNAT. Various randomizations of the sequence for SL3 were performed maintaining the same length as SL3 but changing the sequence content. The randomized sequence was then added to the 5' end of SL4 (**Figure 4.3**), keeping the sequence of SL4 constant. Interestingly, it appeared that in most randomizations (4.3B-4.3E, 4.3G-4.3K) the SL4 formed its main structure with the exception of 4.3F. Therefore, it appears that the RNAT will form its predicted structure regardless of the sequence content of SL3.

A

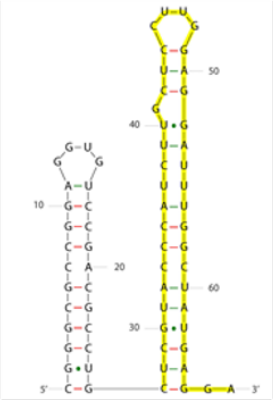

B

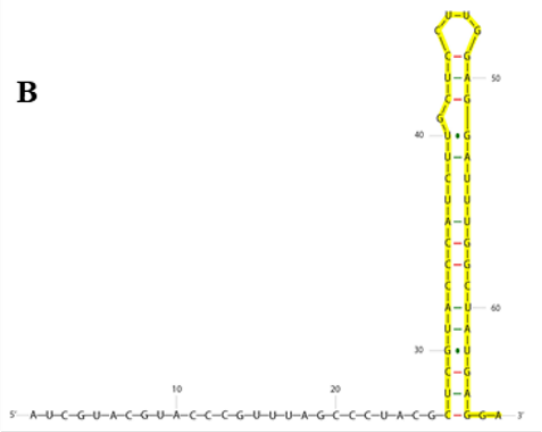

C

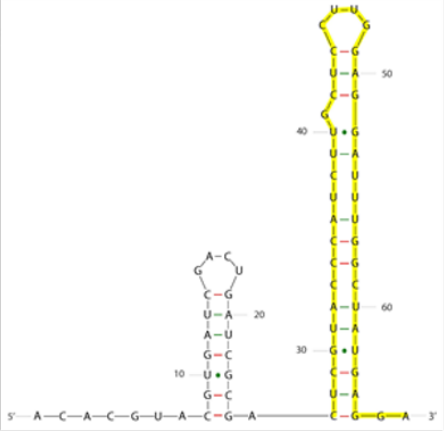

D

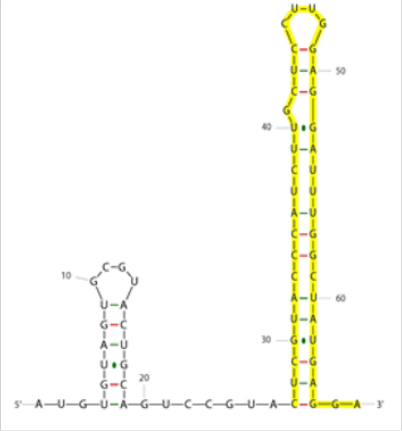

E

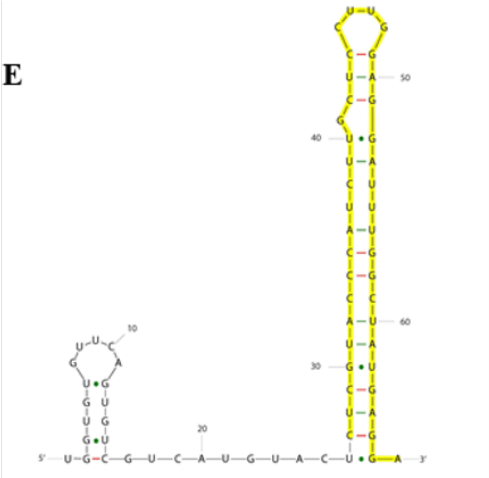

F

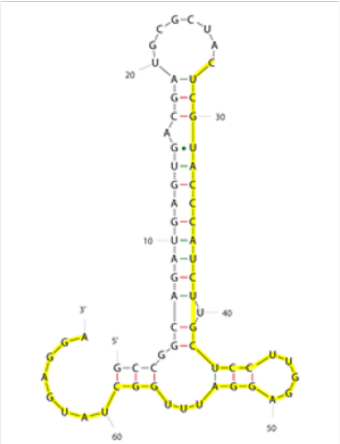

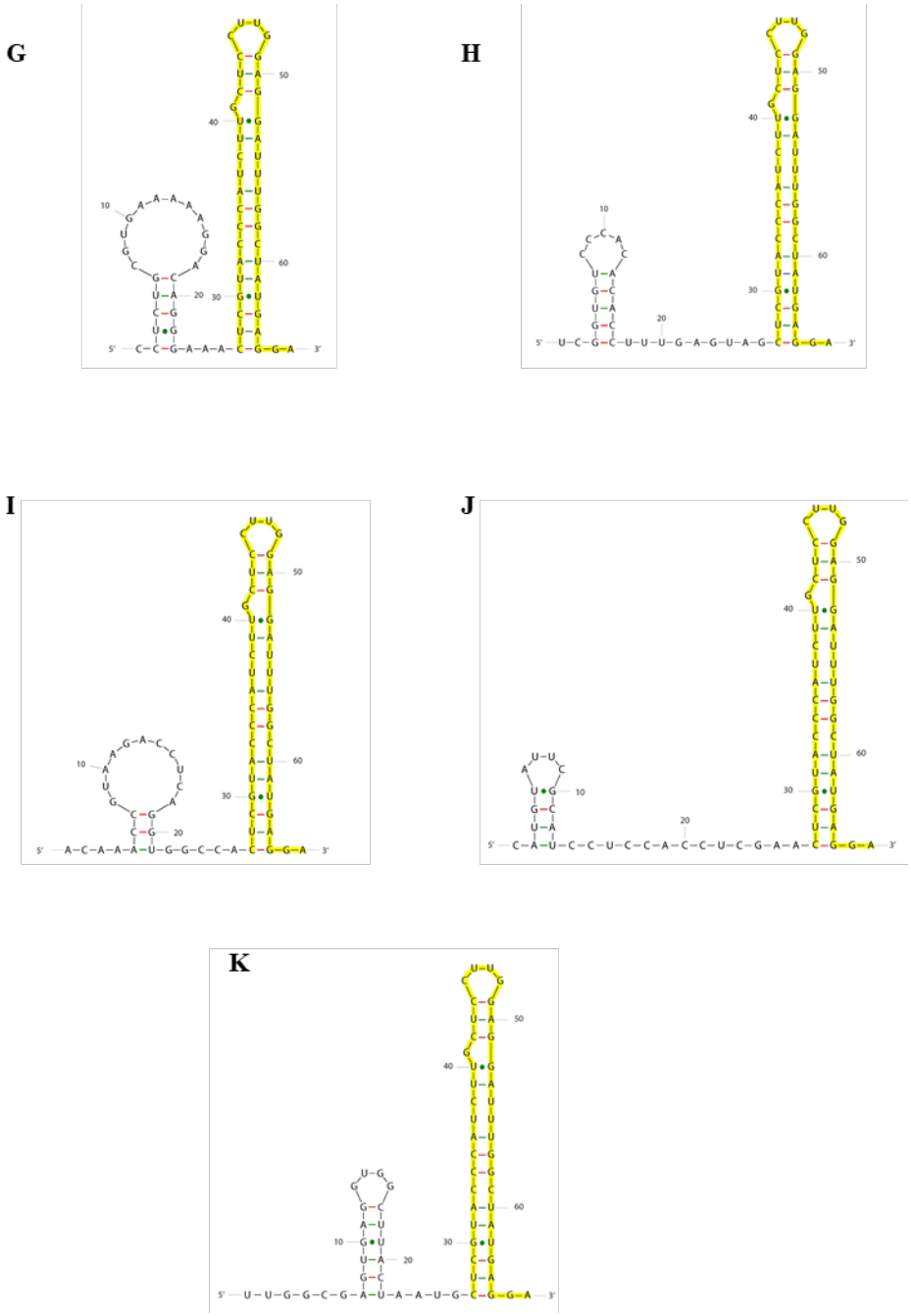

Figure 4.3 Secondary structure predictions of RNAT with randomized sequence of 26 nucleotides added to the 5' end. The secondary structure predictions were prepared using mfold[17] for the A) WT SL3-SL4 sequence, B) Randomization 1, C) Randomization 2 D) Randomization 3, E) Randomization 4, F) Randomization 5 G) Randomization 6, H) Randomization 7, I) Randomization 8, J) Randomization 9, and K) Randomization 10. The SL4 sequence is highlighted in yellow.

To test if disruption of SL1 and SL2 would influence the folding of SL4, randomizations of the same length as the sequence for SL1-SL2 and the spacer between SL2 and SL3 were prepared and added to the 5' end of SL3-SL4 (**Figure 4.4**), keeping the sequence of SL3 and SL4 constant. Secondary structure predictions showed that the SL4 hairpin formed the native structure ~60% (4.4D-4.4E, 4.4G, & 4.4I-4.4K). For these cases, there was at least two hairpin loops preventing interaction with the SL4 sequence. The remaining randomizations disrupted the preferred structure of SL4 (4.4B, 4.4C, 4.4F, & 4.4 H) and showed less base-pairing with the Shine-Dalgarno (SD) sequence. Therefore, the folding of SL1-SL2 into proper stem-loops seems important for the formation of the preferred RNAT structure.

A

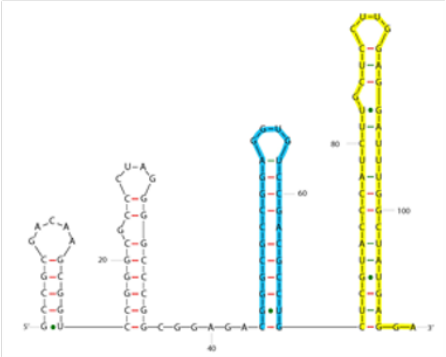

B

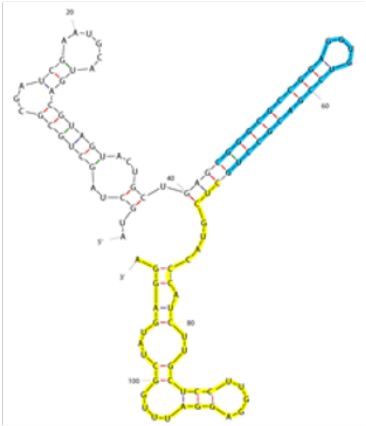

C

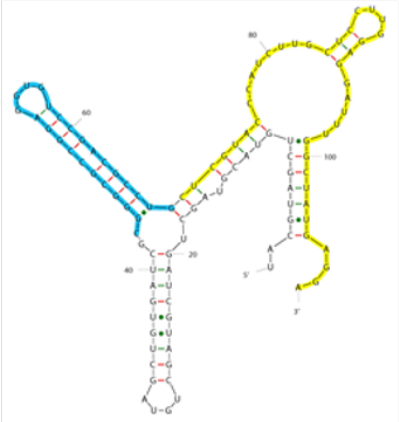

D

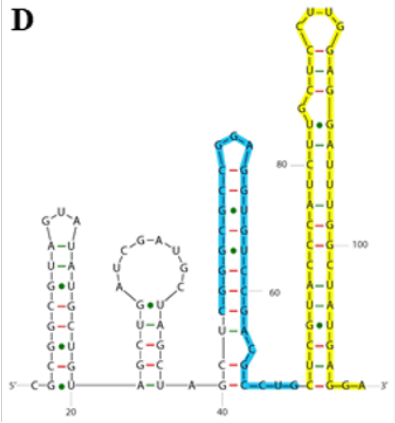

E

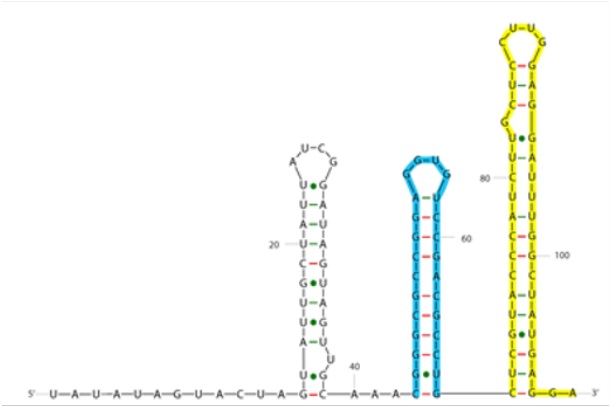

F

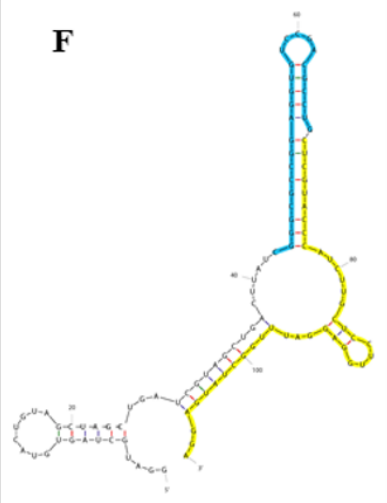

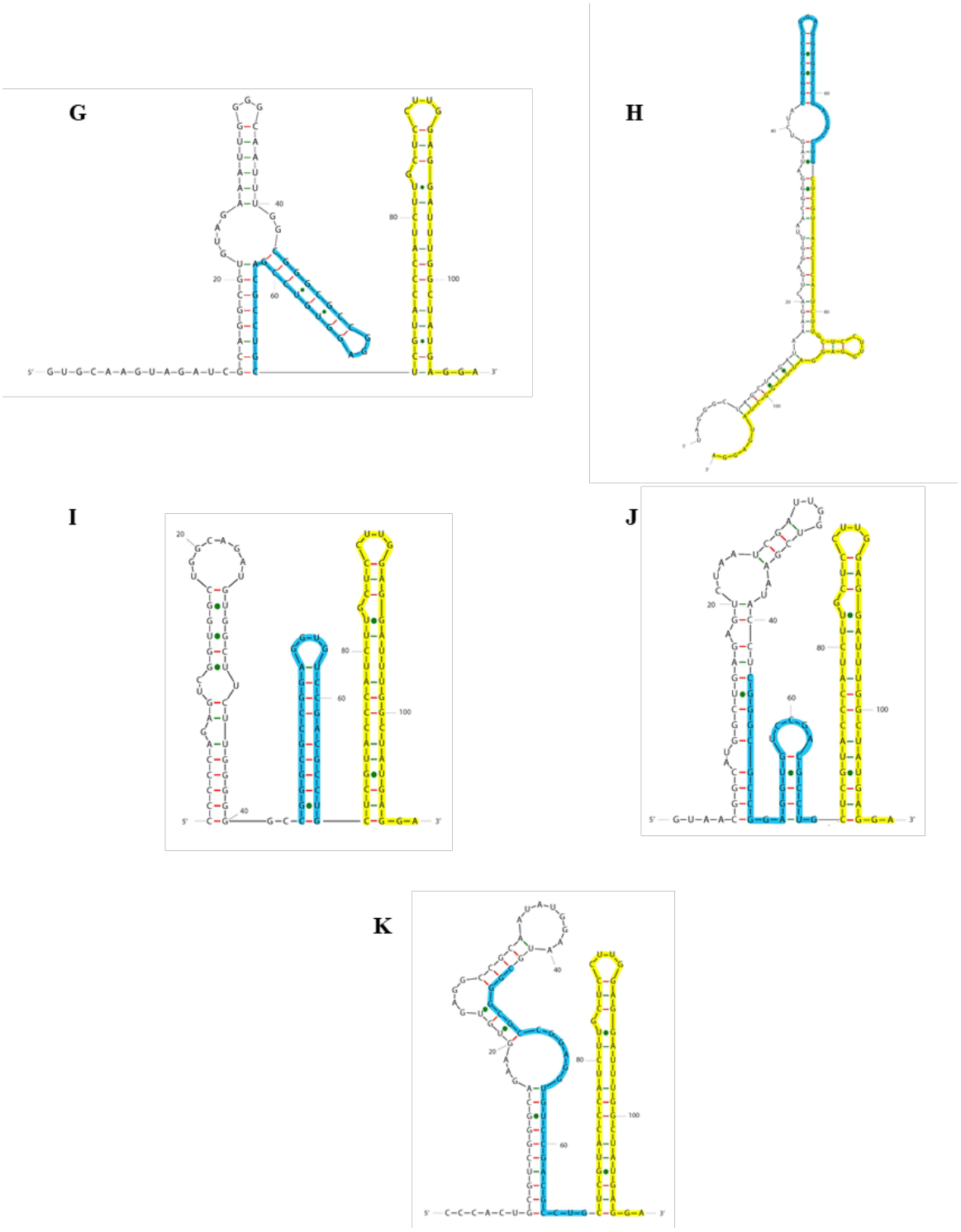

Figure 4.4 Secondary structure predictions of SL3 & SL4 with upstream randomized sequence of 42 nucleotides. The secondary structure predictions were prepared using mfold[17] for the A) WT sequence, B) Randomization 1, C) Randomization 2 D) Randomization 3, E) Randomization 4, F) Randomization 5 G) Randomization 6, H) Randomization 7, I) Randomization 8, J) Randomization 9, and K) Randomization 10. The SL4 sequence is highlighted in yellow and the SL3 sequence is highlighted in blue.

Since the RNAT was significantly less likely to form the correct structure when everything upstream of SL3 is mutated, and because the non-base paired nucleotides between SL2 and SL3 prevented Sl4 from forming a wrong stem-loop initially in transcription (**Figure 4.2**); it appears as if the spacer nucleotides may have a large influence on the SL4 predicted structure. Therefore, randomizations the same length as the SL1 and SL2 hairpins were added onto the 5' end of the sequence for the 6 nucleotide spacer, SL3, and SL4 (**Figure 4.5**). SL4 formed the natural stem-loop structure ~70% (4.5C-4.5E, 4.5G-4.5H, & 4.5J-4.5K). The remaining randomizations did not have an intact SL4 structure (4.5B, 4.5F, & 4.5I) when the 6-nucleotide spacer between SL2 and SL3 began to base-pair with the first nucleotides in SL4.

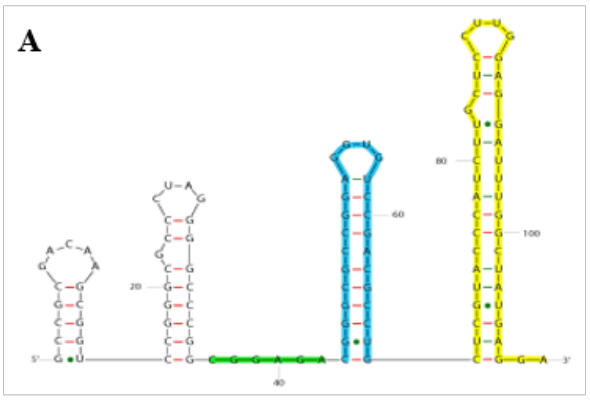
A


B

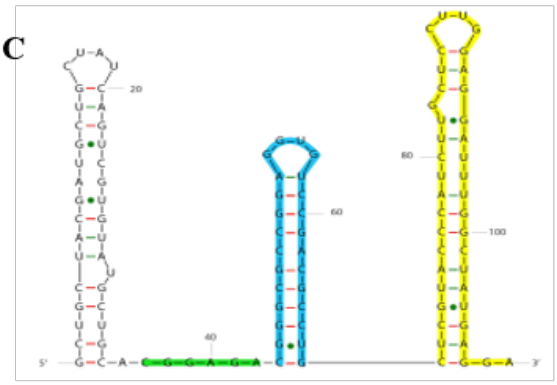
C

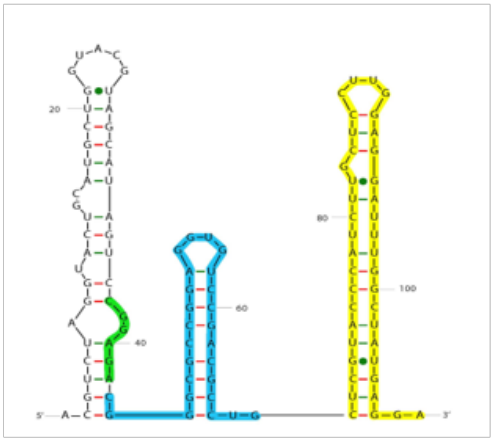
D

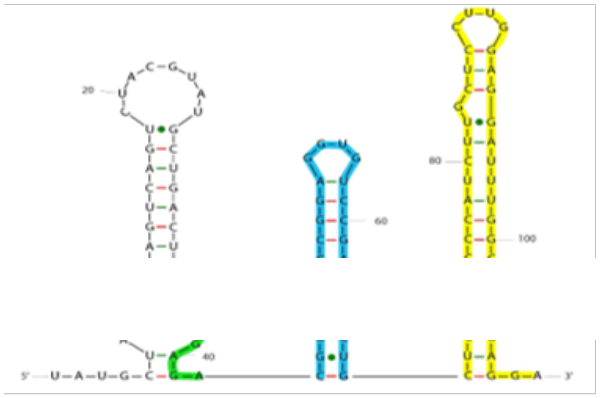
E

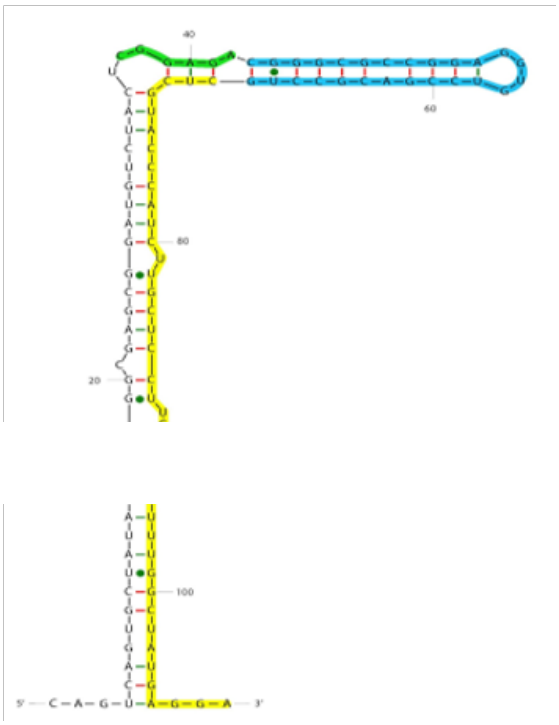
F

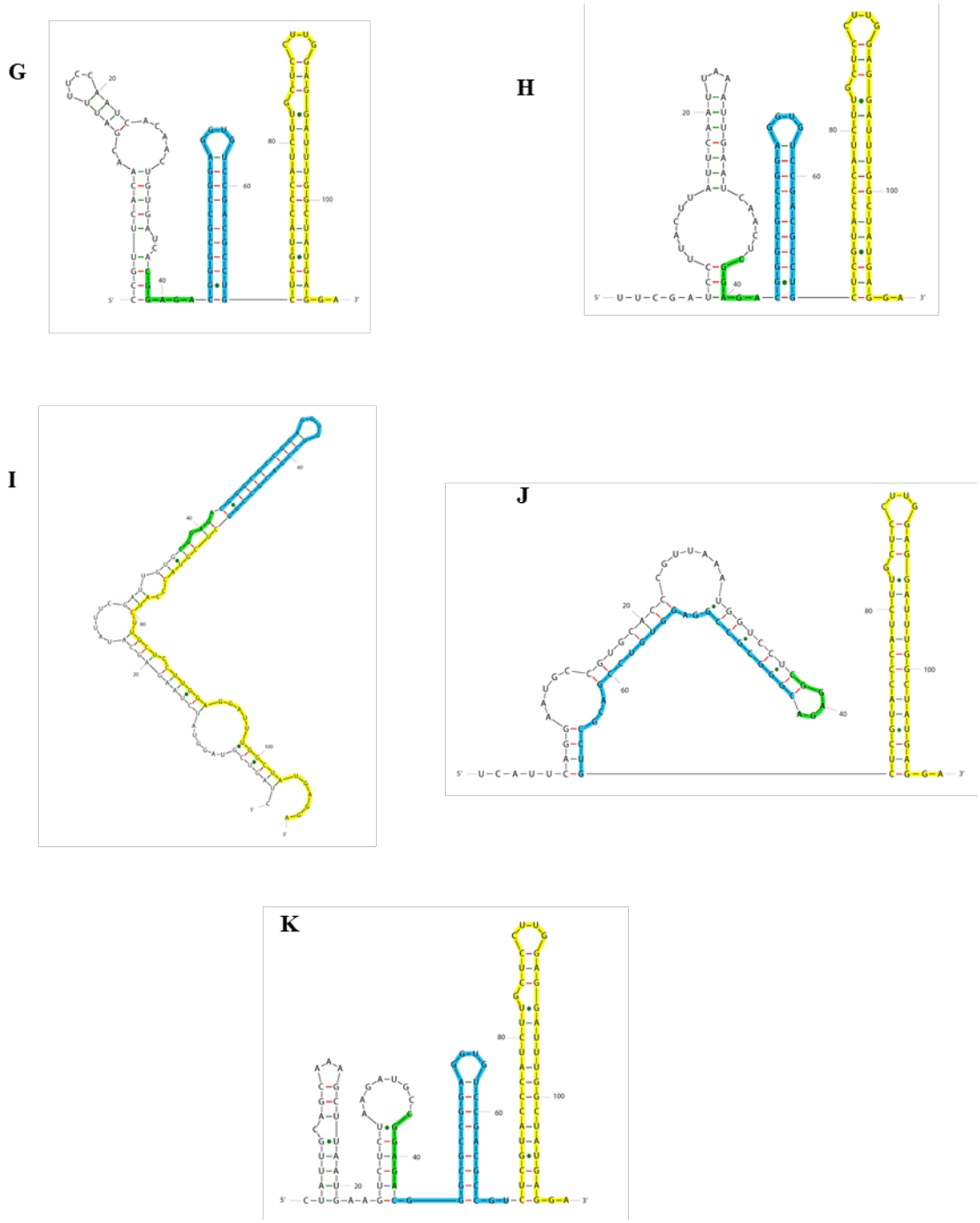

Figure 4.5 Secondary structure predictions of upstream randomized sequence of 36 nucleotides with the 6 nucleotide spacer, SL3, SL4. The secondary structure predictions were prepared using mfold[17] for the A) WT sequence, B) Randomization 1, C) Randomization 2 D) Randomization 3, E) Randomization 4, F) Randomization 5 G) Randomization 6, H) Randomization 7, I) Randomization 8, J) Randomization 9, and K) Randomization 10. The SL4 sequence is highlighted in yellow, the SL3 sequence is highlighted in blue, and the 6 nucleotide non base-paired sequence is highlighted in green.

To further investigate the effect of the spacer, all stem-loop sequences were kept constant and the sequence of the spacer was randomized (**Figure 4.6**) Again, a majority of structures appeared to favor the formation of the correct SL4 (4.6B, 4.6D, 4.6E, & 4.6G-4.6K). Unexpectedly, in the two structures that did not form the correct SL4 (4.6C & 4.6F), it was due again to the spacer base-pairing with the SL4 sequence. Therefore, it seems highly likely that the secondary structure of the upstream hairpins may prevent the 6 not base-paired nucleotides from interacting with SL4.

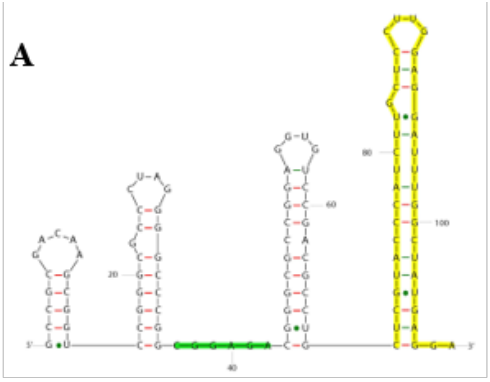
A

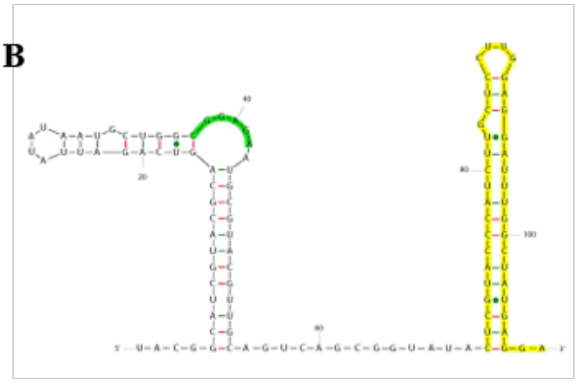
B

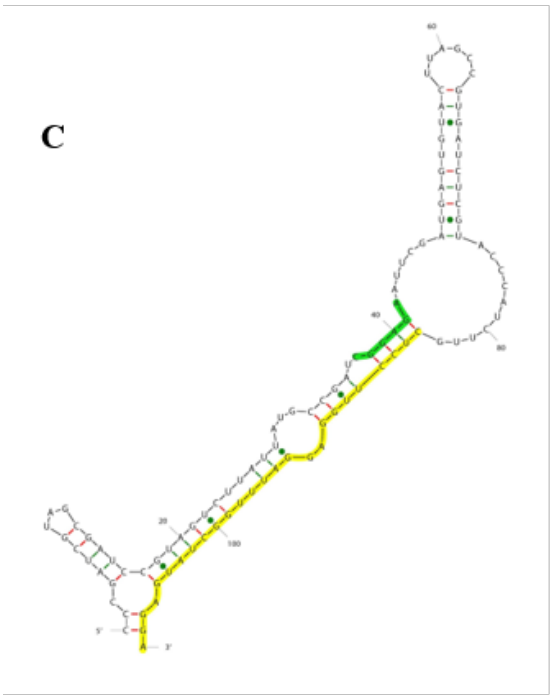
C

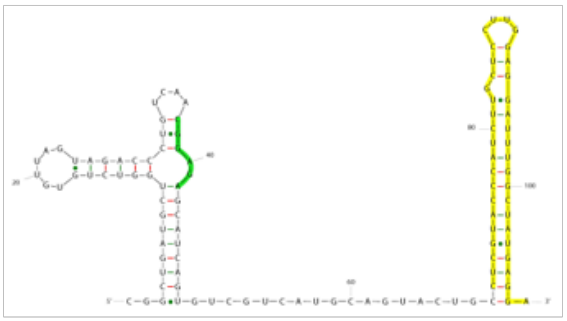
D

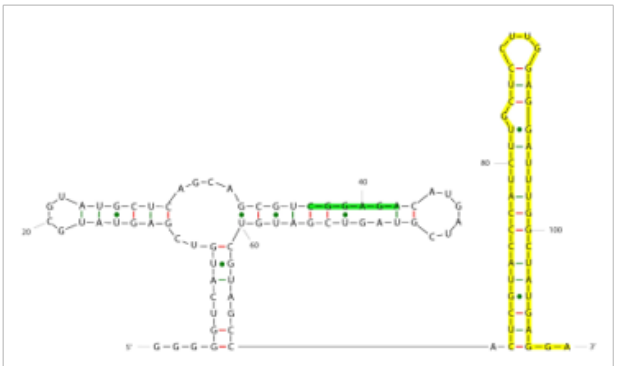
E

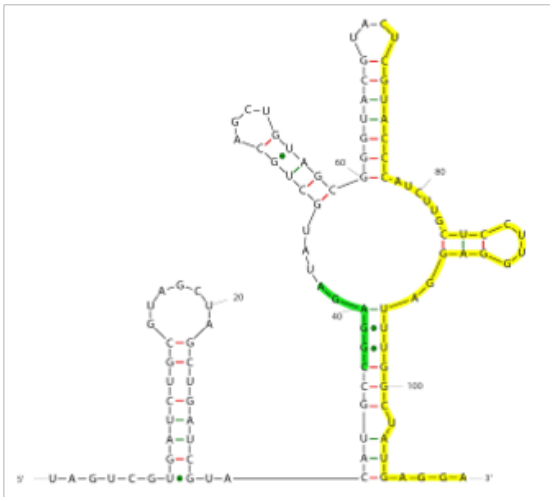
F

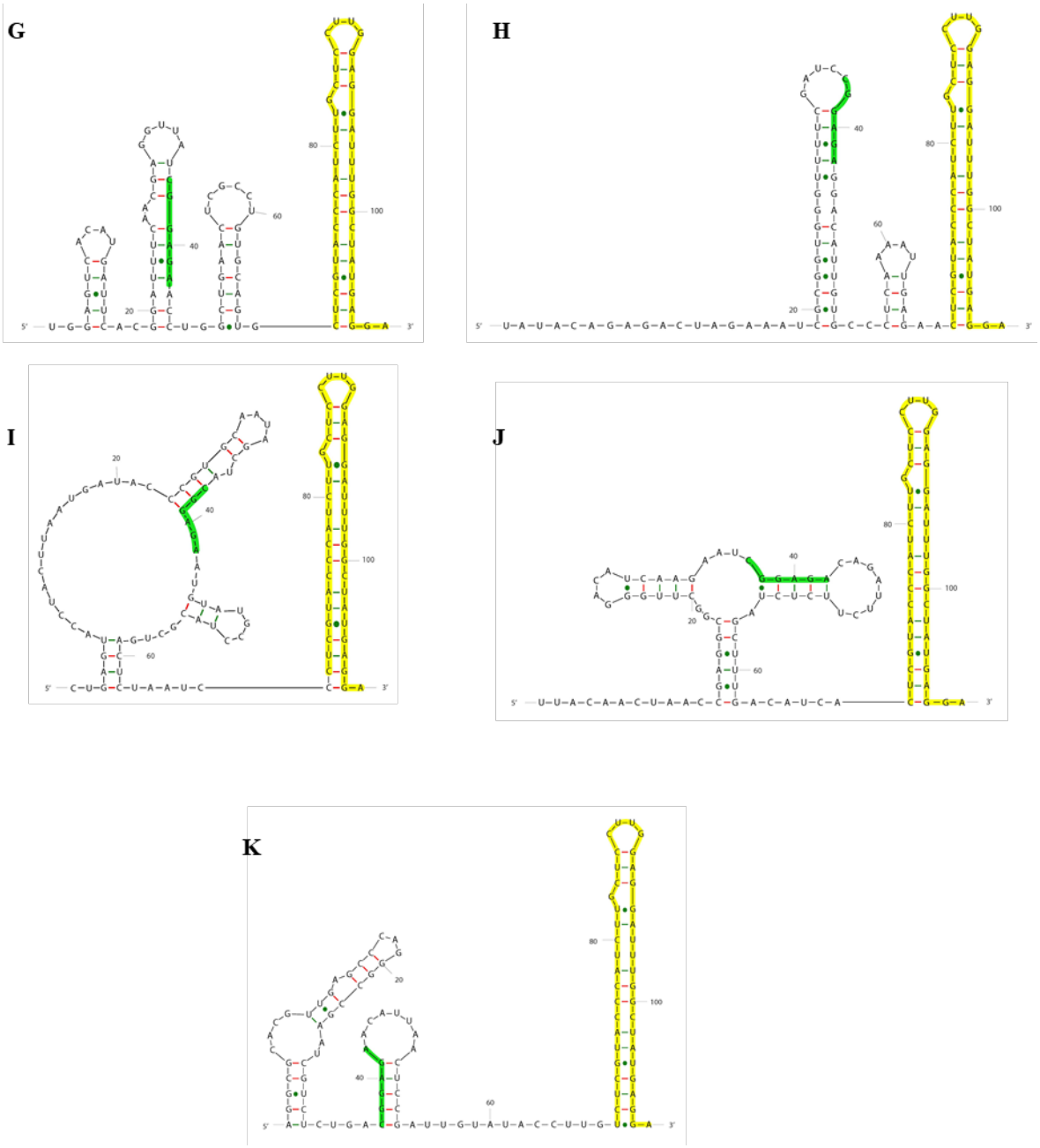

Figure 4.6 Secondary structure predictions of 6 nucleotide spacer& SL4 with randomized sequence of 36 nucleotides added to the 5' end and randomized sequence of 26 nucleotides added between spacer and SL4. The secondary structure predictions were prepared using mfold[17] for the A) WT sequence, B) Randomization 1, C) Randomization 2 D) Randomization 3, E) Randomization 4, F) Randomization 5 G) Randomization 6, H) Randomization 7, I) Randomization 8, J) Randomization 9, and K) Randomization 10. The SL4 sequence is highlighted in yellow and the 6 nucleotide non base-paired sequence is highlighted in green.

Chapter 5

Conclusions and Future Work

The UV thermal denaturation experiments performed demonstrated that the full-length wild-type sequence did not melt in a two-state fashion and had multiple transitions at all the Mg^{2+} concentrations; however, the RNA becomes more thermally stable with increasing Mg^{2+}. Furthermore, the melt data showed that the upstream hairpins are more thermally stable and the upstream hairpins do not assist with the melting of the RNAT. To further validate this point a C59A mutant, which disrupted base-pairing in the immediate upstream stem-loop did not influence the RNAT melting but did cause the upstream hairpins to melt in two-state fashion. However, since *B. japonicum* is a mesotherm, it is improbable that it would ever experience temperatures as high as 50°C, which is the T_m of the RNAT. Therefore, it is more likely that only part of the thermometer melts to allow the ribosome access to the SD sequence and the other hairpins might function to help protect the RNAT from 5' exonucleases until the ribosome can bind.

Knowing that the upstream hairpins do not influence the melting of the RNAT, the next hypothesis was that they influenced the folding of the thermometer. A computational study that randomized the sequence at various locations within the WT sequence was conducted to look at how the upstream sequence influenced the folding of the RNAT. From the data, it appears that the 6-nucleotide spacer between the second and third 5' proximal hairpins in the ROSE element that is not base paired in the WT structure is very important for the RNAT to fold properly. In fact, in the randomizations where the RNAT did not form its natural structure, the 6-nucleotide spacer was base pairing to nucleotides within the SL4. Therefore, the upstream hairpins may be

evolutionarily designed to form their stable structures to allow for the spacer sequence to regulate proper folding of the RNAT.

To determine how the RNAT melts on a more molecular level in order to allow the ribosome access, future studies are being directed at determining the reactivity of the individual nucleotides in the RNAT as temperature changes. This will be accomplished using in-line probing to determine the flexible, and therefore less stable regions within the full length untranslated region. Furthermore, to determine if the folding of the thermometer is dependent on the spacer sequence more extensive computational studies containing a bigger sample size should be conducted. Finally, to determine if the trends seen in *B. japonicum* is an evolutionally conserved feature of ROSE elements, the computational study focused on looking at ROSE elements within other organism will be expanded to include extremophiles.

Appendix A

UV Thermal Denaturation Melts Absorbance at 260 nm

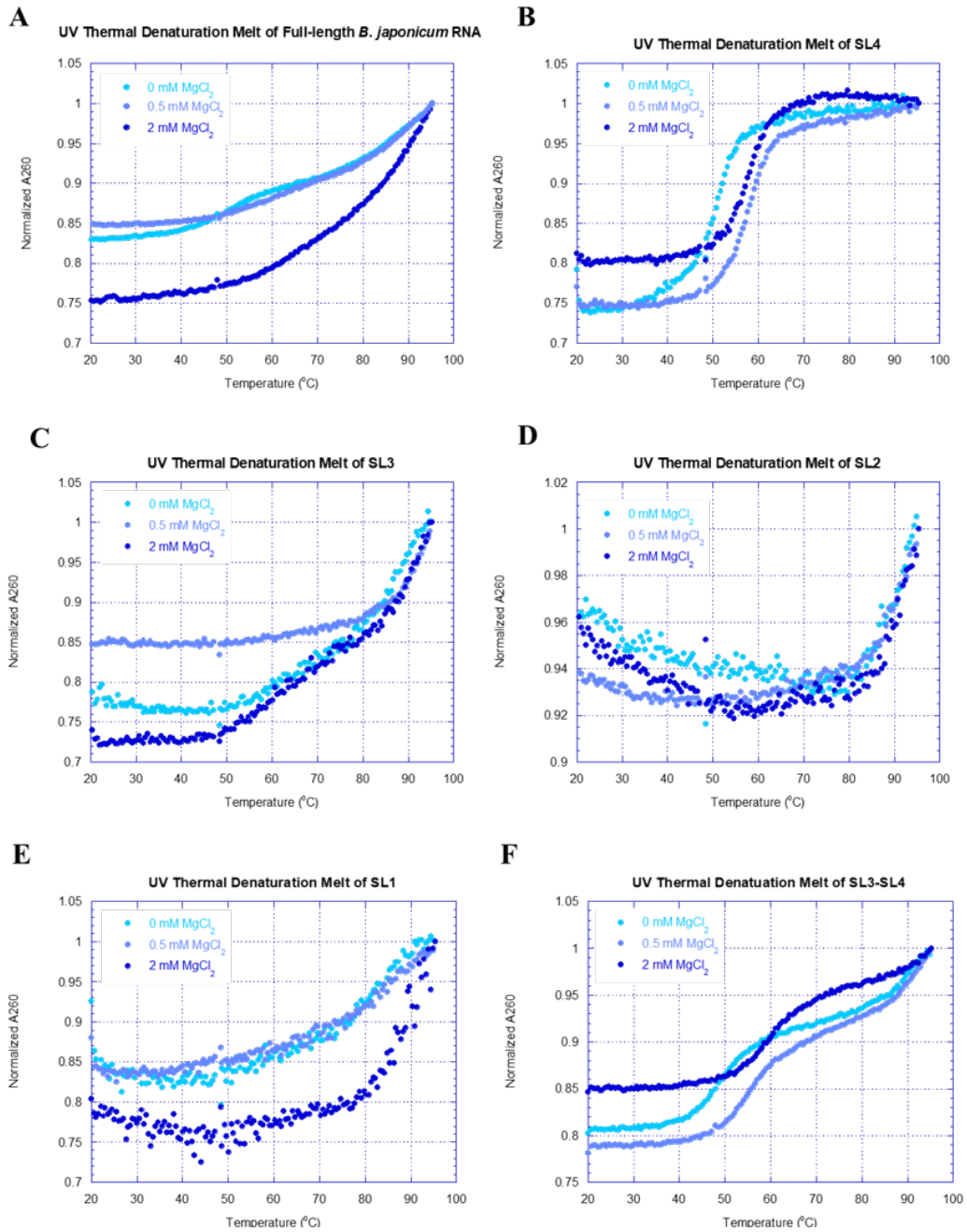

UV thermal denaturation absorbance curves at A260 for the A) full-length 5' UTR of *B. japonicum,* individual RNA stem-loops B) P, C) SL3, D) SL2, and E) SL1, and the F) SL3-SL4 construct. Each curve was the representative data chosen to represent each condition and was normalized to itself.

Appendix B

Simulated Melt Curve Equations

$$A = A_F f_F + A_u f_u \tag{1}$$

Where A is the absorbance, A_F is absorbance of the folded RNA, A_u is absorbance of the unfolded RNA, f_F is the fraction of folded RNA, and f_u is the fraction of unfolded RNA. f_u is also equivalent to:

$$f_u = 1 - f_F \tag{2}$$

Substituting eq. 2 into eq. 1 yields eq. 3:

$$A = A_u + (A_F - A_u) f_F \tag{3}$$

Furthermore, f_F can be written as

$$f_F = \frac{F}{F+U} = \frac{\frac{F}{U}}{\frac{F}{U}+1} = \frac{K}{K+1} \tag{4}$$

Where F is the amount of folded RNA, U is the amount of unfolded RNA, and K is the equilibrium constant. Using the following thermodynamic equations:

$$\Delta G = \Delta H - T\Delta S \tag{5}$$

$$\Delta G = -RT \ln K \tag{6}$$

Where ΔG is the free energy change, ΔH is the enthalpy change, T is the temperature in Kelvin, and ΔS is the entropy change, the equilibrium constant, K, can be written as:

$$K = e^{\left(-\frac{\Delta H}{RT} + \frac{\Delta S}{R}\right)} \tag{7}$$

Eq. 7 can then be substituted into eq. 4 to give eq. 8:

$$f_F = \frac{e^{\left(-\frac{\Delta H}{RT} + \frac{\Delta S}{R}\right)}}{e^{\left(-\frac{\Delta H}{RT} + \frac{\Delta S}{R}\right)} + 1} \tag{8}$$

Finally, eq. 8 can be combined with eq. 3 to yield eq. 9:

$$A = A_u + (A_F - A_u)\frac{e^{\left(-\frac{\Delta H}{RT} + \frac{\Delta S}{R}\right)}}{e^{\left(-\frac{\Delta H}{RT} + \frac{\Delta S}{R}\right)} + 1} \tag{9}$$

Appendix C

UV Thermal Denaturation Melts Absorbance at 280 nm

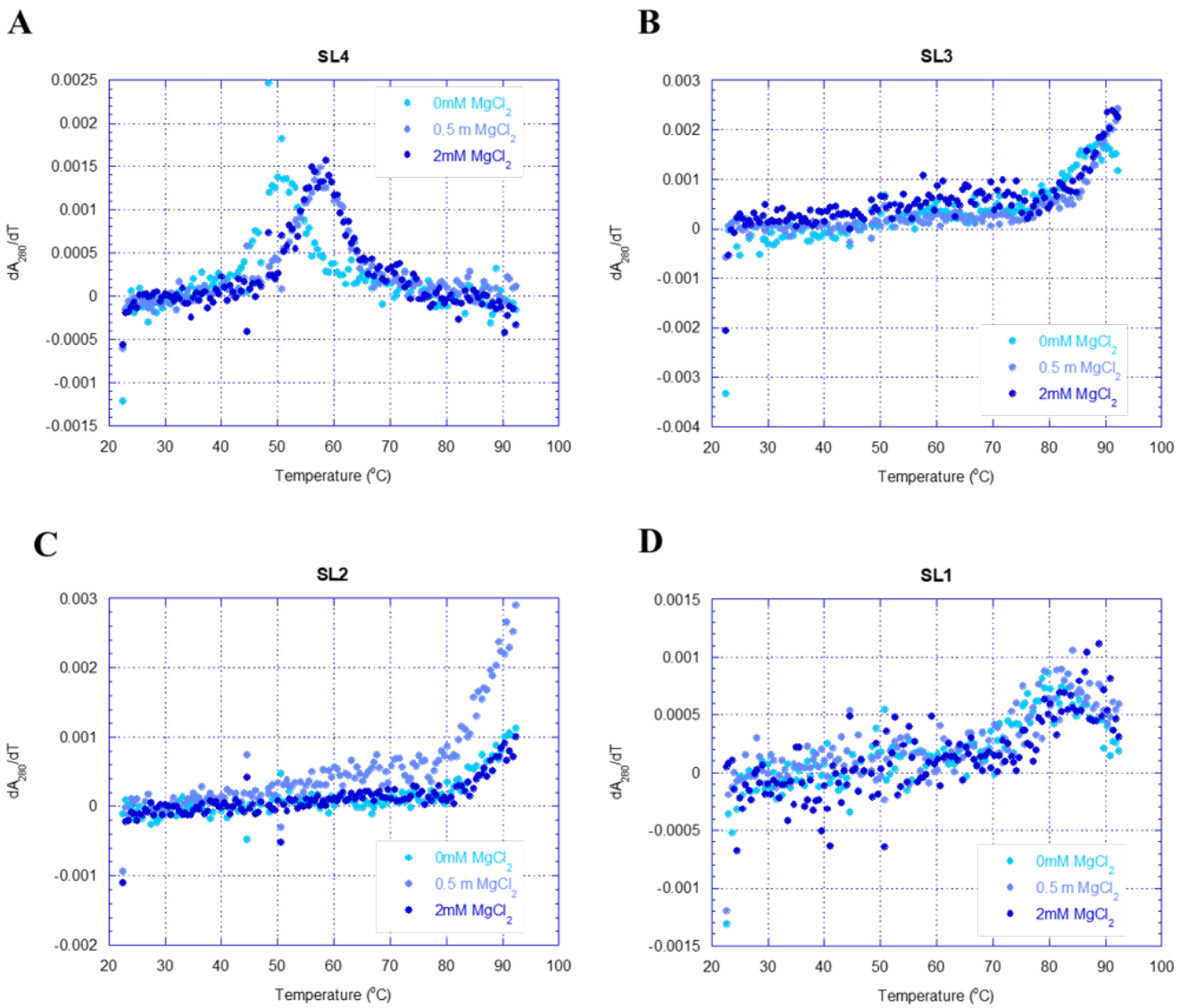

UV thermal denaturation first derivative curves measured at 280 nm of the individual stem-loops A) SL4, B) SL3, C) SL2, and D) SL1 in B. japonicum ROSE element of interest at 0 mM, 0.5 mM, and 2 mM MgCl2.

References

(1) Nudler, E.; Mironov, A. S. The Riboswitch Control of Bacterial Metabolism. *Trends in Biochemical Sciences*. Elsevier Ltd January 1, 2004, pp 11–17. https://doi.org/10.1016/j.tibs.2003.11.004.

(2) Brantl, S. Antisense-RNA Regulation and RNA Interference. *Biochimica et Biophysica Acta - Gene Structure and Expression*. Elsevier May 3, 2002, pp 15–25. https://doi.org/10.1016/S0167-4781(02)00280-4.

(3) Westhof, E.; Filipowicz, W. From RNAi to Epigenomes: How RNA Rules The World. *ChemBioChem* **2005**, *6* (2), 441–443. https://doi.org/10.1002/cbic.200400418.

(4) Rodnina, M. V. Translation in Prokaryotes. *Cold Spring Harbor Perspectives in Biology*. Cold Spring Harbor Laboratory Press September 1, 2018, p a032664. https://doi.org/10.1101/cshperspect.a032664.

(5) Yusupova, G. Z.; Yusupov, M. M.; Cate, J. H. D.; Noller, H. F. The Path of Messenger RNA through the Ribosome. *Cell* **2001**, *106* (2), 233–241. https://doi.org/10.1016/S0092-8674(01)00435-4.

(6) Korostelev, A.; Noller, H. F. The Ribosome in Focus: New Structures Bring New Insights. *Trends in Biochemical Sciences*. Elsevier Current Trends September 1, 2007, pp 434–441. https://doi.org/10.1016/j.tibs.2007.08.002.

(7) Milón, P.; Rodnina, M. V. Kinetic Control of Translation Initiation in Bacteria. *Crit. Rev. Biochem. Mol. Biol.* **2012**, *47* (4), 334–348. https://doi.org/10.3109/10409238.2012.678284.

(8) Chakravarty, S.; Massé, E. RNA-Dependent Regulation of Virulence in Pathogenic Bacteria. *Frontiers in Cellular and Infection Microbiology*. Frontiers Media S.A. October

9, 2019. https://doi.org/10.3389/fcimb.2019.00337.

(9) Gripenland, J.; Netterling, S.; Loh, E.; Tiensuu, T.; Toledo-Arana, A.; Johansson, J. RNAs: Regulators of Bacterial Virulence. *Nature Reviews Microbiology*. December 2010, pp 857–866. https://doi.org/10.1038/nrmicro2457.

(10) Konkel, M. E.; Tilly, K. Temperature-Regulated Expression of Bacterial Virulence Genes. *Microbes and Infection*. Elsevier Masson SAS 2000, pp 157–166. https://doi.org/10.1016/S1286-4579(00)00272-0.

(11) Maleki, F.; Khosravi, A.; Nasser, A.; Taghinejad, H.; Azizian, M. Bacterial Heat Shock Protein Activity. *Journal of Clinical and Diagnostic Research*. Journal of Clinical and Diagnostic Research March 1, 2016, pp BE01–BE03. https://doi.org/10.7860/JCDR/2016/14568.7444.

(12) Kortmann, J.; Narberhaus, F. Bacterial RNA Thermometers: Molecular Zippers and Switches. *Nature Reviews Microbiology*. April 2012, pp 255–265. https://doi.org/10.1038/nrmicro2730.

(13) Narberhaus, F. Translational Control of Bacterial Heat Shock and Virulence Genes by Temperature-Sensing MRNAs. *RNA Biology*. Taylor and Francis Inc. 2010. https://doi.org/10.4161/rna.7.1.10501.

(14) Waldminghaus, T.; Fippinger, A.; Alfsmann, J.; Narberhaus, F. RNA Thermometers Are Common in α- and γ-Proteobacteria. *Biol. Chem.* **2005**, *386* (12), 1279–1286. https://doi.org/10.1515/BC.2005.145.

(15) Krajewski, S. S.; Nagel, M.; Narberhaus, F. Short ROSE-Like RNA Thermometers Control IbpA Synthesis in Pseudomonas Species. *PLoS One* **2013**, *8* (5), e65168. https://doi.org/10.1371/journal.pone.0065168.

(16) Chowdhury, S.; Maris, C.; Allain, F. H. T.; Narberhaus, F. Molecular Basis for Temperature Sensing by an RNA Thermometer. *EMBO J.* **2006**, *25* (11), 2487–2497. https://doi.org/10.1038/sj.emboj.7601128.

(17) Zuker, M. Mfold Web Server for Nucleic Acid Folding and Hybridization Prediction. *Nucleic Acids Res.* **2003**, *31* (13), 3406–3415. https://doi.org/10.1093/nar/gkg595.

(18) Chowdhury, S.; Ragaz, C.; Kreuger, E.; Narberhaus, F. Temperature-Controlled Structural Alterations of an RNA Thermometer. *J. Biol. Chem.* **2003**, *278* (48), 47915–47921. https://doi.org/10.1074/jbc.M306874200.

(19) Transcription in Prokaryotes - The Cell - NCBI Bookshelf https://www.ncbi.nlm.nih.gov/books/NBK9850/ (accessed Feb 16, 2020).

(20) Chamberlin, M.; Mcgrath, J.; Waskell, L. New RNA Polymerase from Escherichia Coli Infected with Bacteriophage T7. *Nature* **1970**, *228* (5268), 227–231. https://doi.org/10.1038/228227a0.

(21) Adlers, S.; Modrichg, P. *T7-Induced DNA Polymerase REQUIREMENT FOR THIOREDOXIN SULFHYDRYL GROUPS**.

(22) Gumport, R. I. EFFECTS OF SPERMIDINE ON THE RNA POLYMERASE REACTION. *Ann. N. Y. Acad. Sci.* **1970**, *171* (3 Metabolism an), 915–938. https://doi.org/10.1111/j.1749-6632.1970.tb39399.x.

(23) Li, Z.; Lau, C.; Lu, J. Effect of the Concentration Difference between Magnesium Ions and Total Ribonucleotide Triphosphates in Governing the Specificity of T7 RNA Polymerase-Based Rolling Circle Transcription for Quantitative Detection. *Anal. Chem.* **2016**, *88* (11), 6078–6083. https://doi.org/10.1021/acs.analchem.6b01460.

(24) Akama, S.; Yamamura, M.; Kigawa, T. A Multiphysics Model of in Vitro Transcription

Coupling Enzymatic Reaction and Precipitation Formation. *Biophys. J.* **2012**, *102* (2), 221–230. https://doi.org/10.1016/j.bpj.2011.12.014.

(25) Ikeda, R. A.; Richardson, C. C. *Interactions of the RNA Polymerase of Bacteriophage T7 with Its Promoter during Binding and Initiation of Transcription*; 1986; Vol. 83.

(26) Nakanishi, S.; Adhya, S.; Gottesman, M.; Pastan, I. Activation of Transcription at Specific Promoters by Glycerol. *J. Biol. Chem.* **1974**, *249* (13), 4050–4056.

(27) Biochemical Roles of Some Essential Metal Ions | Enhanced Reader. *J. Chem. Educ.* **1977**, *54* (12), 761–762.

(28) Lusk, J. E.; Williams, R. J.; Kennedy, E. P. *Magnesium and the Growth of Escherichia Coli*; 1968; Vol. 243.

(29) Truong, D. M.; Sidote, D. J.; Russell, R.; Lambowitz, A. M. Enhanced Group II Intron Retrohoming in Magnesium-Deficient Escherichia Coli via Selection of Mutations in the Ribozyme Core. *Proc. Natl. Acad. Sci. U. S. A.* **2013**, *110* (40). https://doi.org/10.1073/pnas.1315742110.

(30) Romani, A. M. P. Magnesium Homeostasis in Mammalian Cells; 2013; pp 69–118. https://doi.org/10.1007/978-94-007-5561-1_4.

(31) Stein, A.; Crothers, D. M. Conformational Changes of Transfer RNA. The Role of Magnesium(II). *Biochemistry* **1976**, *15* (1), 160–168. https://doi.org/10.1021/bi00646a025.

ACADEMIC VITA

EDUCATION

The Pennsylvania State University – State College, PA
B.S. in Chemistry with honors May 2020
Minor in Biology

HONORS & AWARDS

Sarah Parvin Summer Scholar-
Thomas Jefferson University 2019
- Competitive internship to perform research in ovarian cancer with Jonathan Brody, Ph.D. lab

Evan Pugh Scholar Senior Award-
The Pennsylvania State University 2019
- Academic excellence award

Charles P. and Dorothy A. Neidig Scholarship-
The Pennsylvania State University 2018
- Competitive academic scholarship

Office of Science Engagement Undergraduate Research Fund-
The Pennsylvania State University Fall 2018 & Fall 2019
- Competitive funding for research throughout the academic school year

Joseph A. Dixon memorial Scholarship in Chemistry-
The Pennsylvania State University 2017
- Competitive academic scholarship

President's Freshman Award-
The Pennsylvania State University 2017
- Academic excellence award

Provost Award-
The Pennsylvania State University 2016
- Competitive academic scholarship

Braddock Scholarship-
The Pennsylvania State University 2016
- Competitive academic scholarship

RESEARCH EXPERIENCE

The Pennsylvania State University– State College, PA 2017-Present

- Performed independent research on the effect of RNA secondary structure on the function of a known RNA thermometer. Performed a bioinformatic study focused on the relationship between stability and secondary structure within the 5' UTR of known repression of heat shock gene expression elements.
- Advisor: Philip Bevilacqua, Ph.D. – The Pennsylvania State University

Thomas Jefferson University – Philadelphia, PA 2017-2019

- Assisted postdoctoral researchers and graduate students in research focused on understanding pancreatic and ovarian cancer on a molecular level and exploring novel therapies.
- Advisors: Jonathan Brody, Ph.D. – Thomas Jefferson University

SELECTED POSTERS

- **Bormes, K.**, Jolley, E., Bevilacqua, P., "The Role of RNA Secondary Sturcture in a Known RNA Thermometer from *Bradyrhizobium japonicum"* Rustbelt RNA Meeting; Case Western Reserve University, Cleveland, OH, October 2019 (Poster)
- **Bormes, K.**, Jolley, E., Bevilacqua, P., "The Role of RNA Secondary Sturcture in a Known RNA Thermometer from *Bradyrhizobium japonicum"* ACS 9th Annual Undergraduate Research Symposium; The Pennsylvania State University, University Park, PA, September 2019 (Poster)
- Dhir, T., Schultz, C., O'Hayer, K., **Bormes, K.M.**, Brown, S.,Nevlar, A., Chand, S., Thomsett, H., Jiang, W., Bowers, J., Rhodes, K., Pishvaian, M., Getts, R., Yeo, C.J., Brody, J.R., "Sensitizing pancreatic cancer cells by utilizing targeted siHuR nanotherapy" Philadelphia Academy of Surgeons, Philadelphia, PA, 2018 (Presentation).
- Schultz, C.W., O'Hayer, K., Dhir, T., Bolaji, O., **Bormes, K.M.,** Brown, Z.S., Thomsett, H., Chand, S. Jain, A., Jiang, W., McCarthy, G., Yeo, C.J., Goetz, A., Nevler, A., Brody, J.R., Winter, J.M., Preet, R., Dixon, D., Bowers, J., Rhodes, K., Gettts, R.,"Gaps in the armor: Targeting HuR to sensitize pancreatic cancer" Proceedings of the American Association for Cancer Research Annual Meeting, Chicago, IL, April 2018 (Poster).
- Schultz, C.W., O'Hayer, **Bormes, K.M.,** Dhir, T., Brown, S., Nevlar, A., Chand, S., Thomsett, H., Jiang, W., Bowers, J., Rhodes, K., Pishvaian, M., Getts, R., Brody, J., "Re-sensitizing Pancreatic Cancer, targeted siRNA inhibition of HuR" Proceedings of the AACR-NCI-EORTC International Conference: Molecular Targets and Cancer Therapeutics Philadelphia, PA, Oct 2017 (Poster).

EXTRACURRICULAR ACTIVITIES

Nittany Chemical Society-President for 2019/2020 school year 2016-Present

- President of the student chapter of the American Chemical Society focused on increasing interest in chemistry to the community and promoting professional development of its members.

Alpha Epsilon Delta- Nationally Inducted Member 2016-Present

- National Health Preprofessional Honor Society that encourages excellence in health sciences and is dedicated to giving back to the community.

Emergency Department Volunteer-
Abington Health Lansdale Hospital, Lansdale, PA 2012-2016

- Dedicated 1,126 hours assisting the emergency department staff with cleaning and stocking rooms, creating blood tube packets, and running results and samples to and from the lab. I improved patient morale by transporting patients around hospital and answering general questions. Delivered food and water to patients and improved response time between patients and medical staff.

PHYSICIAN SHADOWING

Internist Huda Abbas, M.D.
Abington Health Lansdale Hospital, Lansdale, PA 2019

- Accompanied Dr. Abbas on her rounds in the hospital

General Surgeon William Bothwell, M.D.
Abington Health Lansdale Hospital, Lansdale, PA 2017

- Observed multiple types of hernia repair surgeries

Pediatric Otolaryngologist Mark Rizzi, M.D.
Children's Hospital of Philadelphia, Chalfont PA 2017

- Observed multiple tonsillectomies, adenoidectomies, and bilateral myringotomies

Pediatric Gastroenterologist Jonathan Flick, M.D.
Children's Hospital of Philadelphia, Chalfont PA 2017

- Observed upper & lower endoscopies and colonoscopies

General Surgeon William Bothwell, M.D.
Abington Health Lansdale Hospital, Lansdale, PA 2014

- Attended office hours and observed outpatient procedures

General Surgeon William Bothwell, M.D.
Abington Health Lansdale Hospital, Lansdale, PA 2013

- Observed a gallbladder surgery and removal of a food bolus

WORK EXPERIENCE

The Pennsylvania State University – State College, PA

- *Biology Department – Senior Learning Assistant* 2018-Present
    - Tutor for students within the course. Responsible for attending lectures, holding weekly office hours, and exam review sessions. Organized other learning assistants within program.